

# A solar-driven 5<sup>th</sup> generation district heating and cooling network with ground-source heat pumps: a thermo-economic analysis

Francesco Calise <sup>a</sup>, Francesco Liberato Cappiello <sup>a,\*</sup>, Massimo Dentice d'Accadia <sup>a</sup>, Fontina Petrakopoulou <sup>b</sup>, Maria Vicedomini <sup>a</sup>

<sup>a</sup> DII - University of Naples Federico II, P.le Tecchio, 80 - 80125 Naples, ITALY

<sup>b</sup> Department of Thermal and Fluid Engineering, Universidad Carlos III de Madrid, Spain



## ARTICLE INFO

### Keywords:

5th generation district heat and cool network  
bidirectional low temperature network  
ground heat pumps  
photovoltaic  
renewable energy district

## ABSTRACT

District Heating and Cooling is considered an efficient solution to address the thermal energy demand of the building sector and reduce its environmental impact. In this paper, a 5<sup>th</sup> generation bidirectional heating/cooling network is designed and modelled. The network is coupled with water-to-water heat pumps, ground heat pumps and a photovoltaic field and is designed to meet the energy requirements of a 50-building district in the city of Leganés (Madrid). All components are modelled in TRNSYS 18. The studied network achieves a primary energy saving index of 64% and reduces the CO<sub>2</sub> emissions by 76% relative to the current situation. The economic analysis of the system results in the relatively long payback period of 33 years, mainly due to the high costs of excavation and the installation of the heat pumps and pipes. With the current design, the photovoltaic field meets only 30% of the electricity demand of the district. However, additional energy storage could help align the power production with the actual power demand better and avoid grid balancing issues. The inclusion of other types of thermal energy consumers would also enhance the performance of the network by increasing the simultaneity between cooling and heating demands.

## 1. Introduction

With climate change affecting the way of living of people all over the world, worldwide Governments are trying to handle the issue implementing different (Tapia et al., 2017, Ye et al., 2021). The European Green Deal (EDG) aims to achieve net zero CO<sub>2</sub> emissions by 2050 (Comission, 2020). The building sector, specifically, is well known for its significant energy consumption and linked to approximately 40% of the total energy demand in Organisation for Economic Cooperation and Development (OECD) Countries (International Energy Agency - IEA 2015). Approximately 50% of a building's primary energy demand is associated with heating, ventilation and air conditioning (HVAC) systems (Pérez-Lombard et al., 2008). The reduction of the energy consumption for space heating and cooling is thus crucial to reduce the environmental impact of the building sector.

District Heating and Cooling (DHC) networks (von Rhein et al., 2019) are considered a suitable, mature (Mahmoud et al., 2020) and environmentally-friendly solution to cover the thermal energy demand of the building sector (Rezaie and Rosen, 2012). A considerable

advantage of DHC networks is the exploitation of low-temperature heat sources from: i) combined heat and power engines (CHP) (Karamanos, 1997); ii) renewable energy sources (solar thermal (Tian et al., 2019, Calise et al., 2020, Calise et al., 2020) and geothermal energy (Carotenuto et al., 2017)); heat pumps (HPs) fed by renewable electricity (photovoltaic (Calise et al., 2020, Calise et al., 2020) or wind (Sinha and Chandel, 2015)); iv) biomass energy (Hammar and Levihn, 2020); v) industrial waste heat (Dénarié et al., 2019). The primary energy consumption and CO<sub>2</sub> emissions of DHC systems can be further reduced by improving the thermal performance of building envelopes (Arriazu-Ramos et al., 2021). Arriazu-Ramos et al. found an average increase of the indoor temperature, mainly in colder periods that additional significant energy and economic savings can be achieved when the system is with a suitable regulation system to prevent overheating. Space heating demand can be also be reduced by implementing a demand-supply optimization (Romanchenko et al., 2021). The positive effect of such a strategy can be further enhanced when suitable energy storage systems are included. Innovative seasonal storage has also been seen to increase the use of renewable thermal energy sources (Saloux and Candanedo, 2020). An example is reported by Todorov et al. (Todorov et al., 2020),

\* Corresponding author.

E-mail address: [francescoliberato.cappiello@unina.it](mailto:francescoliberato.cappiello@unina.it) (F.L. Cappiello).

<b>Nomenclature</b>	
A	area ( $\text{m}^2$ )
C	specific cost-price ( $\text{€}/\text{kWh}$ or $\text{€}/\text{m}^2$ or $\text{€}/\text{m}$ or $\text{€}/\text{t}$ )
$c_p$	specific heat at constant pressure ( $\text{kJ kg}^{-1} \text{K}^{-1}$ )
EER	energy efficiency ratio (-)
G	incident solar total radiation ( $\text{W m}^{-2}$ )
$C_{\text{inv}}$	capital cost (€)
COP	coefficient of performance (-)
J	energy purchasing/selling cost ( $\text{€}/\text{kWh}$ $\text{€}/\text{Sm}^3$ )
LHV	lower Heating Value ( $\text{kWh Sm}^{-3}$ )
$m$	mass flow rate ( $\text{kg s}^{-1}$ )
$m_{\text{plant}}$	plant annual maintenance (%/year)
$m_{\text{PV}}$	PV annual maintenance (%/year)
$N_p$	number of people (-)
$N_{\text{par}}$	number of modules in parallel (-)
$N_s$	number of modules in series (-)
NPV	net present value (€)
P	electric power (kW)
PE	primary energy (kWh/year)
PES	primary energy saving (-)
PI	profit index
$\dot{Q}$	thermal power (kW)
SPB	simple pay back (years)
T	temperature ( $^{\circ}\text{C}$ )
U	overall heat transfer coefficient ( $\text{W m}^{-2} \text{K}^{-1}$ )
v	velocity ( $\text{m s}^{-1}$ )
V	volume ( $\text{m}^3$ )
z	depth (m)
<i>Greek Symbols</i>	
$\Delta$	difference (-)
$\epsilon$	long wave emissivity (-)
$\eta$	efficiency (-)
$\rho$	density ( $\text{kg m}^{-3}$ )
$\rho_s$	solar reflectance (-)
<i>Subscripts</i>	
B	referred to boiler
backfill	referred to backfill materials
CB	referred to condensing boiler
cond	condenser
conv	convective
cool	cooling energy
cooling	referred to cooling thermal flow rate/energy
DHW	domestic hot water
DHC	district heating cooling network
district	referred to electric energy demand of the residential district
E	energy
el	electric
evap	evaporator
excavation	referred to drilling/excavation
feed	referred to feeding flow
fromGRID	referred to electric energy withdrawn from national electric grid
GHE	ground heat exchanger
GHP	ground heat pumps
H&C	referred to heat pump for building space heating and cooling
heat	referred to heating energy
heating	referred to heating thermal flow rate/energy
HP	referred to heat pump
in	input/inlet
LOAD	electricity demand
max	maximum
NG	natural gas
NR	neutral ring
out	output/outlet
PS	referred to proposed system
pump	referred to hydronic pump
PV	referred to photovoltaic field
return	referred to return flow
RS	referred to reference system
self	referred to self-consumed electricity
set	setpoint
SW	source water
t	referred to the value of a parameter in time step
th	thermal
toGRID	referred to electricity sent to national grid
Tk	referred to tank
user	user
UW	user water
5 <sup>th</sup> DHC	referred to the 5 <sup>th</sup> generation district heating and cooling network

presenting an aquifer thermal storage coupled with groundwater HPs, operating in both heating and cooling modes. Energy planning is also crucial for implementing suitable strategies to reduce the energy consumption of DHC systems (Zajacs and Borodjinecs, 2019, Ivezic et al., 2020).

Today, DHC network design is dominated by 4<sup>th</sup> generation district heating (DH) networks that are well known for their reliability and maturity (Harney et al., 2020). The feeding temperature for a 4<sup>th</sup> generation DH is around 50–60°C (Harney et al., 2020). Numerous studies on 4<sup>th</sup> generation networks may be found in the literature (Lund et al., 2021). For example, Ref. (Sameti and Haghighat, 2019) proposes a computational optimization model to design a 4<sup>th</sup> generation DH network in an under-construction Swiss residential district. This work proves that the use of a 4<sup>th</sup> DH network may lead to a 40% reduction of the total annualized district cost and a reduction of the equivalent CO<sub>2</sub> emissions by 17%, with respect to conventional technologies. Fabre et al (Fabre et al., 2018) presented a work on DH operation enhancement. They proved that the adoption of a triple-pipe configuration improves the performance of the network, leading to an increase of the renewable

energy rate by 2–5%. Abokersh et al (Abokersh et al., 2020) studied a DH network coupled with solar-assisted HPs. They showed that the solar-assisted HPs led to an 80–83% reduction of the environmental impact, with respect to the conventional technologies. The operative cost of the proposed layout ranged between 59.1 €/MWh to 90.3 €/MWh, depending on the control strategy the district followed. The integration of solar energy in district heating was also studied by Maximov et al. (Maximov et al., 2021). They investigated a solar DH network, with seasonal thermal storage that provides space heating to the users. Dynamic simulations were used to estimate the time-dependent thermal energy demand. The model of the system (including solar collectors, storage, pumps, boilers, etc.) was developed in TRNSYS and an optimization algorithm was used to detect the cost-optimal configuration. Emissions were seen to reduce by 90 % with a capital cost increase of 20 %. Ref. (Xu et al., 2021) presented a new type of a two-supply/one-return, triple-pipe structure to enhance the performance of a DH network. The pipeline of this layout was studied using computational fluid dynamics, CFD and the simulations were performed with ANSYS. This work found that the linear total heat loss

decreased from 24.13 W/m to 20.16 W/m when the distance between the two water-supply pipes was reduced from 0.114 m to 0.084 m. Finally, Ref. (Gu et al., 2019) analyzed the reduction of the electricity demand of the hydronic systems with variable speed pumps.

Although several studies dealing with 4<sup>th</sup> generation DHC networks are found in literature, some critical aspects and limitations must be noted. In particular, one of the main disadvantages of such networks is that the energy generation is centralized and may thus reduce the network adaptability and efficiency (Abugabbara et al., 2020). With the aim to develop more efficient decentralized DHC networks, increasing attention has been paid to 5<sup>th</sup> generation networks in the past few years (Buffa et al., 2019), (von Rhein et al., 2019). 5<sup>th</sup> generation networks are based on a so called natural feeding temperature that may range between -5°C and 35°C (Buffa et al., 2019). Given the relatively low feeding temperature, this kind of networks are have low conversion losses (Nielsen et al., 2021) and are suitable to be coupled with: i) very low temperature waste heat (data centers (Khosravi et al., 2021), metro stations (Sandvall et al., 2021), and wastewater treatment systems (Nielsen et al., 2020)). Such features can lead to a significant reduction of the primary energy consumption in residential districts (Allen et al., 2020).

The general definition of 5<sup>th</sup> generation districts includes several network configurations, namely: i) Cold District Heating Networks (Pellegrini and Bianchini, 2018) (in German Kalte Nahwärme (Wirtz et al., 2020)); ii) Bidirectional Low Temperature Networks (Bünning et al., 2018); iii) Aenergy Networks (Eicker, 2018) (in German Anergie-netze (Wirtz et al., 2020)). Ref. (Sommer et al., 2020) developed a one-loop bidirectional low-temperature network, where a single loop acts as cold/hot sink, meeting the heating/cooling energy demand of several users. This layout exploited the water of the neutral ring for providing cooling energy. Despite its low complexity, this arrangement is not flexible from a thermodynamic balance point of view. Calixto et al. (Calixto et al., 2021) also modeled an existing neutral-temperature DH network in Ospitaletto (Italy). The system was equipped with decentralized HPs and industrial waste heat and aquifer wells at about 25°C and 15°C, respectively, were used as heat sources. The operation of the network over one year was modeled with both a detailed and an approximate model. In the detailed model the values of operating parameters were calculated. The approximate model was focused on energy balances aggregating all users with a lumped demand. The inputs of the models were the load profiles, while the main outputs were the energy balances and primary energy consumptions. Considering a reasonable agreement between both models, the seasonal performance factors of 4.2 (detailed model) and 4.5 (approximate model) were obtained (including the HPs and network pumping), with primary energy factors lower than 0.5. Ref. (Bilardo et al., 2021) proposed a one-loop bidirectional low temperature network. This layout was very similar to the one proposed in Ref. (Sommer et al., 2020), adopting, however, HPs to meet the cooling energy demand instead of coupling a heat exchanger with the neutral ring. However, despite the accuracy of the model this layout did not consider that the source side temperatures required by the HP in cooling and heating modes are usually not equal. This layout was thus less flexible than the one proposed in Ref. (Sommer et al., 2020).

Ref. (Zarin Pass et al., 2018) presented the environmental benefits of the adoption of 5<sup>th</sup> generation DHC networks, assessing that high-density districts result in less exergy destruction when compared to low density ones. High-density districts achieve exergy distribution losses of 0.18 kJ/kJ-load, while low-density districts result in a value of 0.3. Ref. (Revesz et al., 2020) proposed a novel concept of a smart energy grid based on a 5<sup>th</sup> generation DHC network and electric mobility. In particular, the authors of this paper developed a smart control strategy, expected to better exploit the renewable energy sources for reducing the environmental impact of this smart energy grid. The proposed solution reduced the carbon emissions of the district and of private mobility by 80%. Moreover, Wahlroos et al. (Wahlroos et al., 2017)

studied the use of waste heat of a data center as a suitable source for 5<sup>th</sup> generation DHC networks, showing promising results. Ref. (Wirtz et al., 2021) carried out an optimization analysis to detect the cost-optimal network temperature. This work assessed that a mixed-integer linear program is a suitable control tool to optimally manage the operation of a 5<sup>th</sup> generation DHC network.

Millar et al. (Millar et al., 2021) presented an analysis for determining the operational, economic and carbon benefits of energy-sharing networks driven by HPs for an urban district. The Integrated Energy System Virtual Environment software was used to generate the heating, cooling and hot water loads of the urban district. The obtained loads were used in a multi-objective Mixed Integer Linear Programming optimization method to produce operational curves with minimum costs and emissions for a pool of delocalized HPs. The developed analysis also allowed the identification of buildings performing better when coupled to thermal-energy sharing. The main result was that energy sharing may be enhanced with thermal storage, due to the generally poor simultaneity of heating and cooling demands. In fact, the simulated scenarios with thermal storage showed up to 82% shared energy utilization, compared to the scenarios without thermal storage that resulted in 40% shared energy utilization. They also showed that the Levelised Cost of Energy and carbon emissions may be reduced by 69% and 13%, respectively, with energy sharing networks when compared to electrified non-shared energy systems.

As mentioned before, a 5<sup>th</sup> generation DHC network may use the ground as a thermal energy source, by means of ground heat pumps (GHP). The exploitation of low enthalpy geothermal energy has been proven to achieve significant primary energy savings in the building sector (Chen et al., 2021). In particular, a GHP, which consists of a water-to-water HP coupled with a ground heat exchanger (Yang and Lee, 2020), is a suitable device for addressing a building's thermal energy demand with low energy and environmental impact (Han et al., 2021). Zhou et al (Zhou et al., 2020) analyzed several aspects of residential GHPs. However, they pointed out that this technology was still very expensive when compared to conventional air-cooled HPs. Drilling and piping costs represent the major share of the investment cost of GHP plants. In Ref. (Zhou et al., 2020), a drilling cost of 8–15 €/m was estimated. Ref. (Aditya et al., 2020) proves the high capital and operating cost of such a GHP plant and the authors tried to detect hybrid solutions to reduce its operating cost. This work proposed the concept of hybrid GHP. In a hybrid GHP, a conventional GHP provides the base thermal load, while the peaks of the thermal load are met by conventional technologies.

In Table 1 a comparison between the work presented in this paper and other relevant studies found in literature is shown.

This literature review pointed out the growing interest on 5<sup>th</sup> generation DHC networks. However, despite this high interest in 5<sup>th</sup> generation DHC networks, several points remain unknown and require further consideration. A very limited number of works analyze the energy performance of such networks, using a detailed approach and based on dynamic simulations. In addition, there is currently no study in literature that analyzes a 5<sup>th</sup> generation DHC network, based on bidirectional loops, photovoltaic collectors, and GHPs dynamically. Furthermore, designers of 5<sup>th</sup> generation DHC networks need suitable energy and economic simulation tools, to select the best layout configuration and the optimal values of both design and operating variables. To the best of the authors' knowledge, there is currently no design guidelines published in literature (Wirtz et al., 2020, Ruesch and Evins, 2014).

The present study aims to address the mentioned knowledge gaps and present the dynamic modeling and evaluation of a 5<sup>th</sup> generation bidirectional low-temperature DHC network, coupling GHPs and a photovoltaic field. The studied network includes a warm and a cold ring and constitutes one of the most promising configurations for DHC networks (Wirtz et al., 2020). The proposed layout is selected mainly because HPs, operating in cooling/heating modes, show different rated

**Table 1**

Content comparison of reviewed papers in literature with this work.

Reference	DH/DHC network	5 <sup>th</sup> generation DHC network	Dynamic modeling	Bidirectional loop	Ground heat pumps	Other heat pumps
Present paper	X	X	X	X	X	X
(Arriazu-Ramos et al., 2021)	X	-	-	-	-	-
(Romanchenko et al., 2021)	X	-	X	-	-	X
(Saloux and Candaleno, 2020)	X	-	X	-	-	-
(Todorov et al., 2020)	X	-	-	-	X	-
(Zajacs and Borodinecs, 2019)	X	-	X	-	-	-
(Ivezic et al., 2020)	X	-	-	-	-	X
(Harney et al., 2020)	X	-	-	-	-	-
(Sameti and Haghigat, 2019)	X	-	-	-	-	-
(Fabre et al., 2018)	X	-	X	-	-	-
(Abokersh et al., 2020)	X	-	X	-	X	-
(Maximov et al., 2021)	X	-	X	-	-	-
(Xu et al., 2021)	X	-	-	X	-	-
(Gu et al., 2019)	X	-	-	-	-	-
(Khosravi et al., 2021)	X	-	-	-	-	X
(Sandvall et al., 2021)	X	-	X	-	-	X
(Nielsen et al., 2020)	X	-	X	-	-	X
(Allen et al., 2020)	-	X	-	X	-	X
(Wirtz et al., 2020)	-	X	X	X	-	X
(Bünnig et al., 2018)	X	-	X	X	-	X
(Sommer et al., 2020)	X	-	X	X	-	X
(Calixto et al., 2021)	X	-	X	-	X	-
(Bilardo et al., 2021)	-	X	X	X	-	X
(Zarin Pass et al., 2018)	-	X	X	X	-	X
(Revesz et al., 2020)	-	X	-	X	X	-
(Wahlroos et al., 2017)	-	X	X	-	-	X
(Wirtz et al., 2021)	-	X	X	X	-	X

source/load operating temperatures, according to manufacturer data. Therefore, the HPs balancing the rings and the HPs installed on the user side may operate with higher coefficient of performance. This arrangement is less simple and more expensive but, at the same time more flexible than the one-loop bidirectional low-temperature network studied in (Calixto et al., 2021). Furthermore, the network proposed here is more effective than one-loop bidirectional low-temperature networks with HPs (e.g., network in (Zarin Pass et al., 2018)), in handling sharp variation of the users load.

In summary, the main novelties, and strengths of the present work are the following:

- Detailed characterization of the residential district of Leganes (Madrid, Spain) and careful assessment of the dynamic thermal energy and power demand. The evaluation of detailed time-dependent energy demands is crucial to achieve reliable and accurate simulation results.

- Development of a dynamic simulation tool for a 5<sup>th</sup> generation DHC network for the selected residential district, based on bidirectional loops.
- Dynamic analysis of the integration of water-to-water GHPs and photovoltaic collectors in the proposed 5<sup>th</sup> generation DHC network.
- Dynamic analysis of the thermal energy and power performance of the proposed renewable 5<sup>th</sup> generation DHC network.
- Economic analysis of the proposed renewable network.
- Development of guidelines for the proposed renewable 5<sup>th</sup> generation DHC.

## 2. System Layout

Fig. 1 presents the layout of the 5<sup>th</sup> generation district heating cooling network developed in this work. The system is based on two main neutral rings with HPs designed to meet the space heating/cooling and domestic hot water demand of the selected residential district. As mentioned, the network has a double-ring bidirectional arrangement, considered one of the most promising configurations for these types of

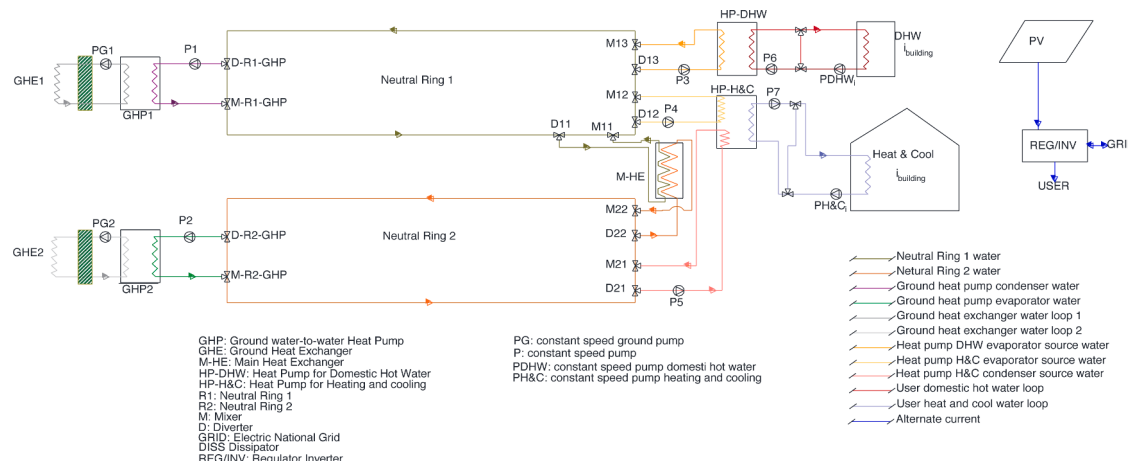


Fig. 1. 5<sup>th</sup> generation DHC network based on ground heat pumps.

applications. In addition, it is equipped with a PV field (2.51 MW peak power) that supplies part of the electricity of the district, demanded by electrical appliances in the buildings and the pumps and HPs of the DHC network.

Neutral Ring 1 (NR1) supplies heat to the evaporators of the HPs for domestic hot water (HPs-DHW) and for building space heating (HPs-H&C). According to available literature, the temperature of this ring ( $T_{NR1}$ ) ranges between 15.5°C and 19°C (Fig. 2). The temperature of NR1 is kept within this range with thermal energy provided to a HP condenser water loop (GHPCW) by a group of 4 ground HPs (GHP1s in Fig. 1) of 1.25 MW<sub>th</sub>/HP. When the  $T_{NR1}$  decreases below 15.5°C, pump P1 is turned on, allowing the GHP1s to supply thermal energy to NR1 until the  $T_{NR1}$  reaches the set point temperature of 19°C (Fig. 2). The water-to-water HPs of GHP1s exchange thermal energy with the ground through a ground heat exchanger water loop 1 (GHEW1). GHEW1 includes the water flowing from the evaporators of GHP1s to the ground heat exchanger GHE1. When GHP1s are in operation, pump PG1 is activated allowing heat exchange between GHEW1 and the ground. The ground is a very performing “hot energy source”, with a rather stable and higher temperature with respect to the outdoor air temperature. This selection is expected thus to increase the COP of the GHP1s, compared to a conventional air-to-water HP.

Neutral Ring 2 (NR2) is designed to provide cooling energy to the condensers of the HPs-H&C, operating in cooling mode. The temperature ( $T_{NR2}$ ) of NR2 ranges between 20°C and 23.5°C (Fig. 2). NR2 is cooled by a group of 2 ground HPs (GHP2s) of a rated capacity of 1.14 MW<sub>th</sub>/HP. GHP2s operate thus in cooling mode, reducing the temperature of NR2 (Fig. 2). The GHP evaporator water loop (GHPEWL) includes the water flowing between NR2 and the evaporators of GHP2s. When GHP2s are in operation, pump P2 is turned on, supplying water from NR2 to the evaporators of GHP2s. The water-to-water GHP2s use the ground as a cold energy source and reject heat to the ground by means of the ground heat exchanger water loop 2 (GHEW2). GHEW2 consists of the water flowing from the GHP2s condensers to the heat exchanger GHE2, where the heat exchange takes place. When GHP2s are in operation, pump PG2 is switched on, pumping GHEW2 water from GHE2 to the condensers of GHP2s. The COP of GHP2s is expected to be enhanced relative to a conventional air-to-water HP operating in cooling mode, since the ground is at an averagely constant and lower temperature with respect to the outdoor air temperature in the summer.

The HPs-DHW loop includes evaporators driven by a group of 4 HPs

supplied by the water delivered from NR1. The user domestic hot water loop (UDHW) consists of the water delivered to the building from the HPs to match the demand for domestic hot water. The domestic hot water (DHW) exploited by the users is then generated by means of a heat exchanger.

UDHHL consists of 4 branches. The operating temperature of the UDHW ( $T_{UDHW}$ ) ranges from 46°C to 55°C (Fig. 3). When the temperature of UDHW falls below 46°C, the HPs-DHW are activated. Pump P3 is switched on to deliver the water of NR1 to the HPs-DHW, which supply thermal energy to UDHW, until the  $T_{UDHW}$  reaches 46°C. When HPs-DHW are in operation, P6 is also turned on. Conversely, when there is some thermal demand for DHW, the pump PDHW<sub>i</sub> is activated, allowing the branches of UDHW to meet the DHW demand.

The HP H&C loop consists of 4 main branches and includes the water loop delivering thermal energy from NR1 to 4 HPs-H&C of 1.25 MW<sub>th</sub>, operating in heating mode. The thermal demand for building space heating of the buildings of the district is met by the H&C water loop (UHCW). The temperature of this loop ( $T_{UHCW}$ ) in heating mode operation is designed for ranging from 42°C to 50°C (Fig. 4). When the temperature of UHCW ( $T_{UHCW}$ ) drops below 42°C, the HPs-H&C are activated, until  $T_{UHCW}$  rises above 50°C (Fig. 4). Pump P2 is switched on to allow NR1 water to provide thermal energy to the evaporators of the HPs-H&C. At the same time, pump P7 is activated to discharge the heat produced by HPs-H&C to the UHCW. These branches exchange heat with substations in the buildings that then feed fan coils in the apartments. During the summer period, HPs-H&C operate in cooling mode, and the HPs-H&C are fed water from NR2. The temperature in this case ranges from 10°C to 15°C (Fig. 4). Thus, when the  $T_{UHCW}$  rises over 15°C, HPs-H&C are activated, cooling UHCW. Pump P5 is also activated to allow NR2 water to flow to the condensers of HPs-H&C. HPs-H&C are turned off when the  $T_{UHCW}$  gets below 10°C. When there is some thermal demand for building space heating and cooling, pump PH&C<sub>i</sub> is activated. This allows water to flow into the buildings to meet the thermal demand.

During the summer period, when there is both heating and cooling demand, heat exchanger M-HE allows heat exchange between NR1 and NR2. Thermal energy is transferred from NR2 to NR1, limiting the operation – and the primary energy consumption – of the ground source HPs. M-HE may allow to partly heat NR1, using NR2, simultaneously cooling NR2. This process is thus expected to enhance the thermal energy performance of the overall system.

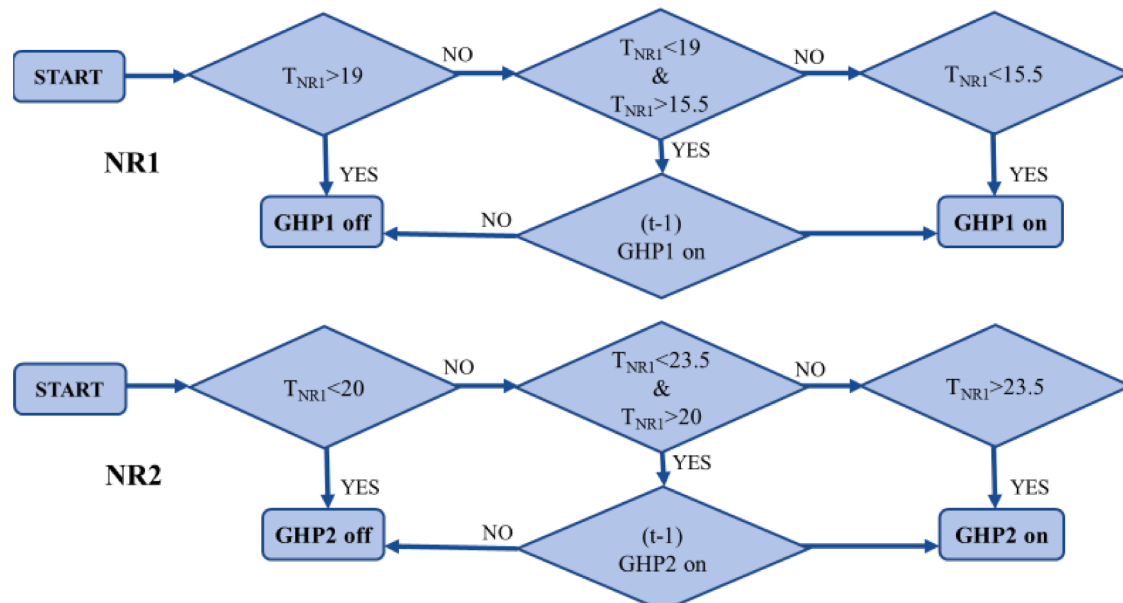


Fig. 2. Neutral Ring 1 (NR1) and Neutral Ring 2 (NR2) control strategy.

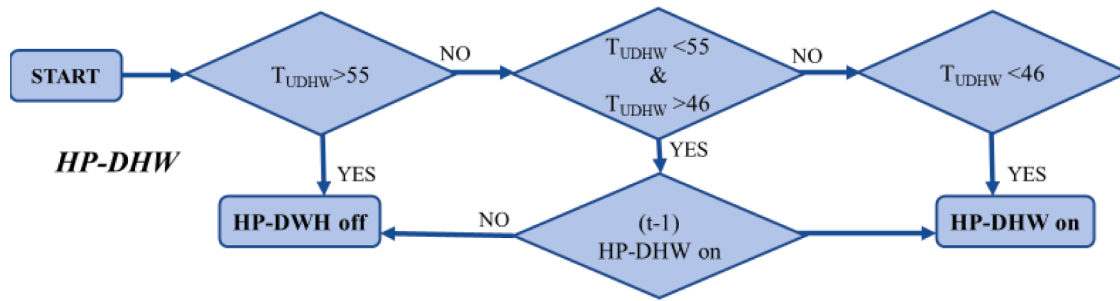


Fig. 3. HPs-DHW operating strategy.

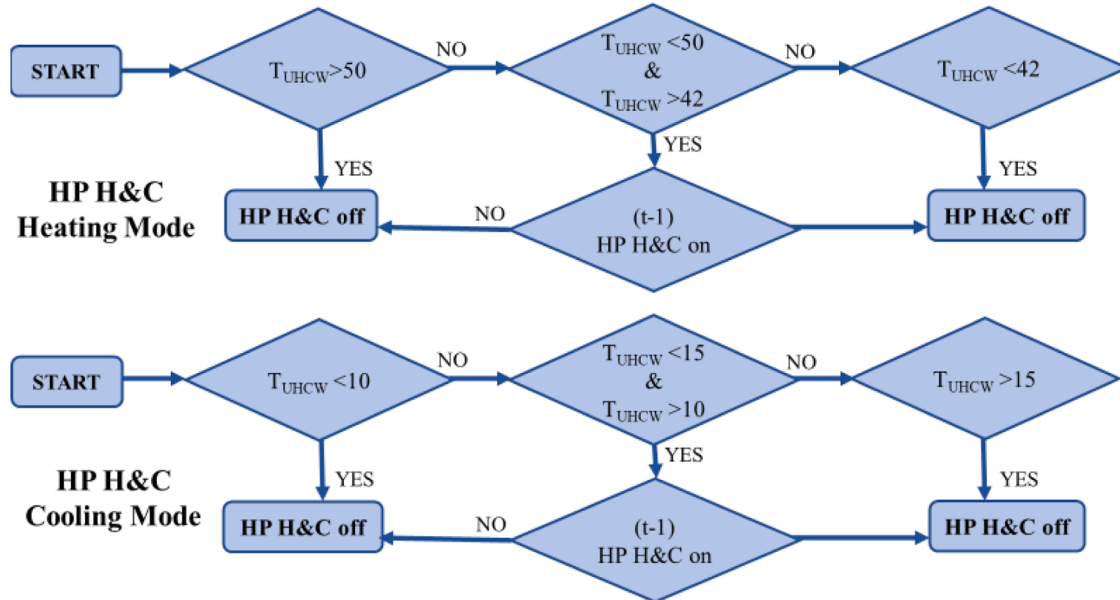


Fig. 4. HP H&amp;C operating strategies.

Lastly, the plant is equipped with a 2.51 MWe PV field. The power produced by the PV field is delivered to the district for meeting of its power demand. The district load consists of i) the power demand for the electrical appliances in the apartments, ii) the power delivered to auxiliary devices of the hydronic systems, and iii) the power delivered to the HPs of the 5<sup>th</sup> generation DHC network.

### 3. System model

The models of the proposed 5<sup>th</sup> generation DHC and the residential district are developed in TRNSYS 18. TRNSYS comes with a large library of components and is widely employed for the evaluation of the dynamic energy performance of solar systems (Buonomano et al., 2013) and the simulation of building energy demand (Calise, 2010). This software allows simulations of real-time operation for a representative year, based on weather data of the Meteonorm database.

The present paper includes detailed models for several components: building, HPs, controllers, diverters, mixers, pumps, ground heat exchangers, heat exchangers, pipes, PV panels, inverter, etc. Type 94 models the photovoltaic panels, consisting of poly-crystalline/crystalline silicon cells (a complete description of the model is provided in Ref. (Calise et al., 2019)). The buildings of the district are modelled with the Google SketchUp TRNSYS3d plug-in (Murray et al., 2009). The 3-D model of the buildings are exported to TRNSYS 18 with library Type 56. Type 56 carefully simulates the building dynamic energy performance, considering: i) the envelope thermophysical properties; ii) the effect that the environment has on the building, i.e.,

ambient temperature, humidity, solar obstruction, and solar radiation; iii) the building 3-D geometry; and iv) the indoor heat gain. This model is considered a reference for the dynamic simulation of buildings and it is often used for the code-to-code validation of user-developed simulation models (Buonomano et al., 2016). Type 556 models the ground heat exchanger based on the Oak Ridge National Labs model (Mei, 1986). This model carefully simulates the heat exchange between the ground and the pipe. In particular, the following main assumptions are considered: i) the heat transfer takes place only along the circumferential path and ii) the heat transfer does not occur along the axis of the pipe. Further details about this model are provided in Ref. (Calise et al., 2020). Table 2 summarizes the main TRNSYS libraries employed in the 5<sup>th</sup> generation DHC network layout developed in this paper.

**Table 2**  
Summary of main components.

Library	Description	Reference
Type 56	Building Model	(Buonomano et al., 2016)
Type 927	Water-to-Water heat pump	present manuscript
Type 94	Photovoltaic panels	(Calise et al., 2019)
Type 21	Hydronic pumps	(Calise, 2010, Lu et al., 2021)
Type 647	Divertor manifold	(Klein et al., 2006, TRNSYS )
Type 649	Mixer manifold	(Klein et al., 2006, TRNSYS )
Type 69	Divertor	(Klein et al., 2006, TRNSYS )
Type 62	Mixer	(Klein et al., 2006, TRNSYS )
Type 64	Cross flow heat exchanger	(Calise, 2010)
Type 556	Ground heat exchanger	(Calise et al., 2020)
Type 31	Pipeline	(Calise, 2010, Lu et al., 2021)

### 3.1. Heat Pump model

Type 927 describes the performance of an electrically driven single-stage water-to-water HP and adopts the normalized catalogue data look-up approach (Handbook, 1996, ASHRAE, 2005). Therefore, the dynamic balances of type 927 are based on performance data maps provided by the manufacturer of the HP.

The HP instantaneous coefficient of performance (*COP*) in heating mode is evaluated as:

$$COP_i = \frac{P_{th,heating,i}}{P_{el,heating,i}} \quad (1)$$

Where,  $P_{th,heating}$  is the thermal energy instantaneously discharged by the HP to the user water (UW), that is the water delivered to the users, and  $P_{el,heating}$  is the power instantaneously used by the HP.

The thermal energy withdrawn from the source fluid is evaluated with Eq. (2)

$$P_{th,fromSW} = P_{th,heating,i} - P_{el,heating,i} \quad (2)$$

Where,  $P_{th,fromSW}$  is the thermal energy, i.e., the heat, withdrawn from the water source (SW).

Finally, the temperatures of the source and user water are evaluated.

$$\begin{cases} T_{SW,out,i} = T_{SW,in,i} - \frac{P_{th,fromSW,i}}{\dot{m}_{SW,i}cp_{SW}} \\ T_{UW,out,i} = T_{UW,in,i} + \frac{P_{th,heating}}{\dot{m}_{UW,i}cp_{UW}} \end{cases} \quad (3)$$

Where,  $T_{SW,out}$  and  $T_{SW,in}$  are the temperatures of the water exiting and entering the HP, respectively,  $\dot{m}_{SW,i}$  is the water flow rate of the source,  $cp_{SW}$  is the specific heat of SW,  $T_{UW,out}$  and  $T_{UW,in}$  are the temperatures of the water exiting and entering the HP, respectively,  $\dot{m}_{UW,i}$  is the water flow rate to the user, and  $cp_{UW}$  is the specific heat of UW.

The COP of the HP operating in cooling mode is estimated as follows:

$$COP_i = \frac{P_{th,cooling,i}}{P_{el,cooling,i}} \quad (4)$$

Where,  $P_{th,cooling}$  is the cooling thermal energy provided by the HP, i.e., the thermal energy withdrawn from the user water, and  $P_{el,cooling}$  is the power absorbed by the HP.

The thermal energy discharged to the source water flow is evaluated as follows:

$$P_{th,toSW} = P_{th,cooling,i} + P_{el,cooling,i} \quad (5)$$

Where,  $P_{th,toSW}$  is the thermal energy discharged to SW.

In conclusion, the temperatures of UW and SW are evaluated as follows:

$$\begin{cases} T_{SW,out,i} = T_{SW,in,i} + \frac{P_{th,toW,i}}{\dot{m}_{SW,i}cp_{SW}} \\ T_{UW,out,i} = T_{UW,in,i} - \frac{P_{th,cooling}}{\dot{m}_{UW,i}cp_{UW}} \end{cases} \quad (6)$$

### 3.2. Thermoconomic model

The energy performance of the residential district and of the proposed renewable 5<sup>th</sup> generation DHC network are assessed through the primary energy (PE) demand of the district and the primary energy saving index (PES).

The primary energy of the reference system (RS), i.e., the residential district, is evaluated as follows:

$$PE_{RS} = \sum_t \left[ \left( E_{el,LOAD} + \frac{E_{th,cool}}{COP_n} \right) \frac{1}{\eta_{el}} + \left( \frac{E_{th,heat}}{\eta_B} + \frac{E_{th,DHW}}{\eta_B} \right) \right]_t \quad (7)$$

Where,  $E_{el,LOAD}$  is the total electricity demand and  $E_{th,heat}/E_{th,cool}$  is the annual thermal energy demand for space heating/cooling. Table 3 displays the remaining terms of this equation.

The primary energy PE of the proposed system is evaluated according to the following equation:

$$PE_{PS} = \sum_t \left[ (E_{el,fromGRID} - E_{el,toGRID}) \frac{1}{\eta_{el}} \right]_t \quad (8)$$

Where,  $E_{el,fromGRID}$  and  $E_{el,toGRID}$  are the electricity withdrawn and delivered to grid, respectively.

In conclusion the PES index is evaluated with Eq. (9).

$$PES_{PS} = \frac{PE_{RS} - PE_{PS}}{PE_{RS}} \quad (9)$$

To evaluate the performance of the 5<sup>th</sup> generation DHC, the following energy saving index is also evaluated:

$$PES_{5thDHC} = \frac{(E_{el,HPs} + E_{el,pumps}) 1/\eta_{el}}{\left( \frac{E_{th,heat}}{\eta_B} + \frac{E_{th,DHW}}{\eta_B} \right) + \frac{1}{\eta_{el}} \frac{E_{th,cool}}{COP_n}} \quad (10)$$

Where,  $E_{el,HPs}$  is the electricity delivered to all of the HPs, and  $E_{el,pumps}$  is the electricity demand of all the auxiliary hydronic systems, i.e.,

**Table 3**  
Thermoconomic and environmental assumptions.

Parameter	Description	Value	Unit
$c_{PV}$	PV unit capital cost per kW <sub>el</sub>	1000 (Buonomano et al., 2018)	€/kW <sub>el</sub>
$c_{pump}$	Cost of the Salmon 240 m <sup>3</sup> /h pump	3.02 (SALMSON 2019)	€/pump
	Cost of the Salmon 150 m <sup>3</sup> /h pump	6.09 (SALMSON 2019)	€/pump
	Cost of the Salmon 110 m <sup>3</sup> /h pump	0.73 (SALMSON 2019)	€/pump
	Cost of the Salmon 100 m <sup>3</sup> /h pump	4.66 (SALMSON 2019)	€/pump
	Cost of the Salmon 100 m <sup>3</sup> /h pump	4.48 (SALMSON 2019)	€/pump
$c_{piping}$	Cost of piping for district heating network	33 (Piemonte, 2018)	€/m
$c_{HP}$	Cost of HP	150 (Calise et al., 2020, Aermec 2020)	€/kW
$c_{excavation}$	Excavation cost	5 (Piemonte, 2018)	€/m <sup>3</sup>
$c_{HFPE, pipe}$	Specific linear cost for HDPE pipe	12.80 (GIORDANO, i. 2020)	€/m
	$r_{GHE} = 0.100 \text{ m}$		
	$r_{GHE} = 0.080 \text{ m}$	8.29 (GIORDANO, i. 2020)	t/€
$c_{backfill}$	Cost for backfill material (sand)	14.45 (Calise et al., 2020)	t/€
$J_{el,fromGRID}$	Electricity purchasing unit cost	0.223	€/kWh
$J_{el,toGRID}$	Electricity selling unit cost	0.05	€/kWh
$J_{NG}$	Natural gas unit cost	0.689	€/Sm <sup>3</sup>
$m_{PV}$	PV maintenance annual cost	1	%/year
$m_{plant}$	Plant maintenance annual cost	0.5	%/year
$LHV_{NG}$	Natural gas lower heating value	9.59	kWh/Sm <sup>3</sup>
$\eta_{el}$	Conventional thermo-electric power plant efficiency	49.8	%
$\eta_B$	Natural gas boiler	75.0	%
$F_{NG}$	Equivalent CO <sub>2</sub> emissions for coefficient for natural gas	0.190 (Calise et al., 2020)	kgCO <sub>2</sub> /kWh <sub>PE</sub>
$F_{el}$	Equivalent CO <sub>2</sub> emissions for coefficient for electricity	0.182 (Neymark and Judkoff, 2008)	kgCO <sub>2</sub> /kWh <sub>el</sub>

pumps.

The annual operating cost ( $C$ ) of the residential district is evaluated as follows:

$$C_{RS} = \sum_t \left[ \left( E_{el,LOAD} + \frac{E_{th,cool}}{COP_n} \right) J_{el,fromGRID} + J_{NG} \left( \frac{E_{th,heat}}{\eta_B} + \frac{E_{th,DHW}}{\eta_B} \right) \right] / LHV \quad (11)$$

Where,  $J_{el,fromGRID}$  is the purchasing cost of electricity and  $J_{NG}$  is the cost of natural gas.

The operative cost of the proposed system also considers the plant maintenance ( $m_{plant}$ ) and the selling cost of electricity ( $J_{el,toGRID}$ ), shown in Table 3.

$$C_{PS} = \sum_t [E_{el,fromGRID} J_{el,fromGRID} - E_{el,toGRID} J_{el,toGRID} + m_{plant}] \quad (12)$$

The annual savings ( $\Delta C_{PS}$ ) are evaluated as follows:

$$\Delta C_{PS} = \frac{C_{RS} - C_{PS}}{C_{RS}} \quad (13)$$

The capital cost ( $C_{inv}$ ) depends on the proposed layout:

$$C_{inv} = C_{HP} + C_{PV} + C_{pumps} + C_{piping} + C_{GHE} \quad (14)$$

$C_{GHE}$  represents the capital cost of the ground heat exchanger, evaluated with Eq. (15).

$$C_{GHE} = c_{excavation} \cdot A_{GHE} + c_{length} \cdot l_{GHE} + c_{backfill} \cdot V_{backfill} \cdot \rho_{backfill} \quad (15)$$

Table 3 and Table 4 summarize the main terms adopted in this equation.

The simple payback period ( $SPB$ ), the net present value ( $NPV$ ) and

**Table 4**  
Ground heat exchanger characteristics (Calise et al., 2020).

Component	Parameter	Description	Value	Unit
GHE1	$l_{GHE}$	Ground heat exchanger length	m	200000
	$r_{GHE}$	Ground heat exchanger radius	m	0.100
	$A_{GHE}$	Ground heat exchanger area	km <sup>2</sup>	0.123
	$V_{backfill}$	Backfill material volume	m <sup>3</sup>	5315
	$h_{conv}$	Flow convection coefficient	W/(K m <sup>2</sup> )	900
	$z_{max}$	Max depth	m	9
	$l_{GHE}$	Ground heat exchanger length	m	100000
GHE2	$r_{GHE}$	Ground heat exchanger radius	m	0.083
	$A_{GHE}$	Ground heat exchanger area	km <sup>2</sup>	0.057
	$V_{backfill}$	Backfill material volume	m <sup>3</sup>	4298
	$h_{conv}$	Flow convection coefficient	W/(K m <sup>2</sup> )	900
	$z_{max}$	Max depth	m	9
	$k_{HDPE}$	Thermal conductivity	W/(m K)	0.49
	$\rho$	Density of the material	kg/m <sup>3</sup>	965
Sand (backfill material)	$c_p$	Specific heat of the material	J/(kg K)	2.25
	$\epsilon$	Roughness	mm	0.3
	$k_{backfill}$	Thermal conductivity	W/(m K)	1.5
	$\rho_{backfill}$	Density of the material	kg/m <sup>3</sup>	1500
Clay (ground)	$c_{p,backfill}$	Specific heat of the material	J/(kg K)	1798
	$k_{ground}$	Thermal conductivity	W/(m K)	0.862
	$\rho_{ground}$	Density of the material	kg/m <sup>3</sup>	1430
	$c_{p,backfill}$	Specific heat of the material	J/(kg K)	1439

the profit index ( $PI$ ) are calculated to assess the economic performance of the developed 5<sup>th</sup> generation DHC network.

The environmental analysis is carried out according to the following equations.

$$CO_2RS = \sum_t \left[ \left( E_{el,LOAD} + \frac{E_{th,cool}}{COP_n} \right) F_{el} + \left( \frac{E_{th,heat}}{\eta_B} + \frac{E_{th,DHW}}{\eta_B} \right) F_{NG} \right] \quad (16)$$

$$\Delta CO_{2,PS} = \frac{CO_{2RS} - CO_{2PS}}{CO_{2RS}}$$

Table 3 presents the main terms of this equation.

The effect of the heat exchange between NR1 and NR2 on the performance of the overall DHC network is evaluated with Eq. (17).

$$R_{HPH\&C} = \frac{E_{th,M-HE}}{E_{th,fromHPH\&C}} \quad (17)$$

$$R_{HPDHW} = \frac{E_{th,M-HE}}{E_{th,toHPDHW}}$$

$E_{th,M-HE}$  is the thermal energy transferred to NR1 from NR2 with M-HE,  $E_{th,toHPDHW}$  represents the thermal energy supplied to the evaporators of HPs-DHW, and  $E_{th,fromHPH\&C}$  represents the thermal energy discharged from the condenser of the HPs-H&C operating in cooling mode.

Finally, the demand overlap coefficient (DOC) is evaluated (Wirtz et al., 2020):

$$\Phi = \frac{2 \cdot \sum_t \min(P_{th,Heat,t}, P_{th,Cool,t})}{\sum_t (P_{th,Heat,t} + P_{th,Cool,t})} \quad (18)$$

Where,  $P_{th,Heat,t}$  is the total heating energy demand, including the heat demand for building space heating and DHW, while  $P_{th,Cool,t}$  is the cooling energy demand.

#### 4. Case study

A small district of the city of Leganes (Madrid, central Spain) is selected. The district includes 50 buildings and 2490 inhabitants. The approach reported in Ref (Calise et al., 2020) is adopted to estimate the thermal and electricity demand of the district.

Four representative buildings (Fig. 5, Table 5 and Table 6) are considered for describing the district. The selection of these types of buildings is based on available literature and inspection of the considered residential district. In addition, three types of representative users are selected, namely family of four people (FAM), old people (OP), and young people (YP). Based on a statistical report about Leganes (Instituto Nacional de Estadística, Leganes ayuntamiento), the population of the district has been defined as: i) 64% FAM; ii) 20% couples of OP and iii) 16% four YP living alone, according, Table 5 displays the distribution of each user type for each type of building and Table 6 shows the main features of each type of building selected.

According to the approach reported in Ref. (Calise et al., 2020), heat gain evaluation is a key issue for correctly assessing the thermal energy demand of a district. To model this, each apartment is carefully characterized by defining the occupation of the people inside the apartment (Fig. 6), the electrical appliances installed in each apartment (Table 7), and a usage strategy of these electrical devices (Fig. 7).

The buildings of the RS are built between 1950 and 1970, they are made of brick and are poorly insulated thermally (Casquero-Modrego and Goñi-Modrego, 2019). Table 8 summarizes the thermophysical characteristic of the selected buildings. The domestic hot water demand is estimated based on the regulation UNI-EN-ISO-13790 (Maximov et al., 2021). The heating period is from September 16<sup>th</sup> to April 30<sup>th</sup>, while the cooling period is between May 1<sup>st</sup> and September 15<sup>th</sup> (Leganes ayuntamiento) (Table 6). The set point temperature for the heating period

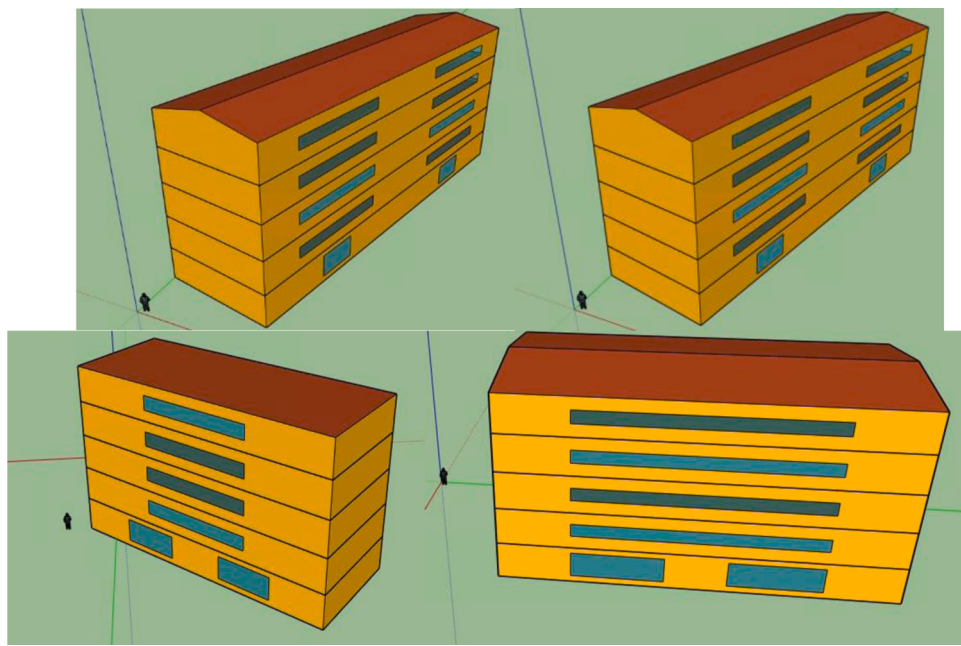


**Fig. 5.** Building geometric 3D model.

**Table 5**  
Occupation assumptions of the different building types in the district.

Type of Building	Family	Number of buildings	
		Old people	Young people
A	8	2	2
B	8	2	-
C	8	3	4
D	8	3	2

**Table 6**  
Building simulation assumptions.

Geometric Features	A	B	C	D
Height [m]	15.5	17	15	16
Volume [ $\text{m}^3$ ]	5890	12426	3750	1934
Floor area [ $\text{m}^2$ ]	380	804	250	512
Number of planes [-]	5	5	4	5
Number of apartments for floor [-]	4	8	3	5
Apartment area [ $\text{m}^2$ ]	80	90	70	92
Glass area [ $\text{m}^2$ ]	192	540	136	262
Heating and cooling season	Heating: $T_{\text{set}} = 20^\circ\text{C}$ 16 <sup>th</sup> September-30 <sup>th</sup> April Cooling: $T_{\text{set},\text{residential}} = 27^\circ\text{C} & T_{\text{set},\text{commercial}} = 26^\circ\text{C}$ 1 <sup>st</sup> May-15 <sup>th</sup> September			
Occupancy schedule	<a href="#">Fig. 6</a> <a href="#">Fig. 7</a>			
Daily power load [kW]	0.6			
Air infiltration rate [vol/h]	0.6			
Average daily DHW demand [ $\text{m}^3/\text{day}$ ]	200			
DHW set point temperature [ $^\circ\text{C}$ ]	45			

( $T_{\text{set,heating}}$ ) is assumed equal to  $20^\circ\text{C}$  and for the cooling period ( $T_{\text{set,cooling}}$ ) is assumed equal to  $26^\circ\text{C}$ . The power demand of the district is met by the electric national grid. The building space heating and domestic hot water demand is matched by natural gas fired conventional boilers, with a rated efficiency ( $\eta_B$ ) of 0.75. The space cooling demand is met with electrically driven air-to-air HPs.

The proposed system (PS) includes the proposed 5<sup>th</sup> generation district is based on 14 HWFG6214 AERMEC (Aermec 2020) HPs (Table 9). A certain amount of the power demand of the district is met by a 16090 m<sup>2</sup> PV field. GHE1 consists of a of 200,000 m length piping made of

high-density polyurethane (HDPE), with an overall area of 0.123 km<sup>2</sup>. These pipes are buried at a depth of 9 m. This depth was selected because it is characterized by a more stable ground temperature. In addition, the ground temperature at 9 m depth is suitable for operating the HPs evaporator within the required design range. GHE2 consists of a 100,000 m HDPE piping system, with an overall area of 0.057 km<sup>2</sup>, also installed at a depth of 9 m. The ground is assumed to be clay and a backfill material (sand) is assumed to be installed between the pipes and the ground.

## 5. Results

The used simulation tool returns a large amount of results of the operation of the developed system for an entire representative year. The generated dynamic plots allow the detailed analysis and correct evaluation of the operation of the system and the optimization of the system control strategies. These results can also be evaluated on different time scales. In the following, the results are presented and discussed on a daily, monthly, and annual scale.

### 5.1. Daily Results

**Fig. 8** summarizes the energy performance of the HPs matching the thermal demand of the district for building space heating. The COP of the HPs operating in heating mode ranges between 5.00 and 4.70. These are remarkably higher values compared to COP of conventional air-to-water HPs and higher than the rated COP of the HPs, i.e., 4.67, see Table 9. This is achieved mainly with the relatively high feeding temperature ( $T_{\text{feed,NR1}}$ ) of the NR1 on the source side of the HPs, i.e., the evaporator side. In particular, the feeding temperature ranges between  $15.5^\circ\text{C}$  and  $19^\circ\text{C}$ . Therefore, the HPs may operate at an evaporation temperature much higher than that of conventional air-to-water HPs. It is well known, from thermodynamics, that the higher the evaporation temperature, the higher the COP and the lower the electricity demand. **Fig. 8** shows that the trend of the COP of the HPs is strictly linked to the temperature of NR1 ( $T_{\text{feed,NR1}}$ ) that in turn affects the evaporation temperature of the HPs. For example, from 06:50 to 08:35 am the COP shows a decreasing trend, mainly due to the decrease of  $T_{\text{feed,NR1}}$  from  $19^\circ\text{C}$  to  $15.5^\circ\text{C}$ . However, the COP also decreases for higher values of the condensation temperature. From 08:30 am, the COP continues to

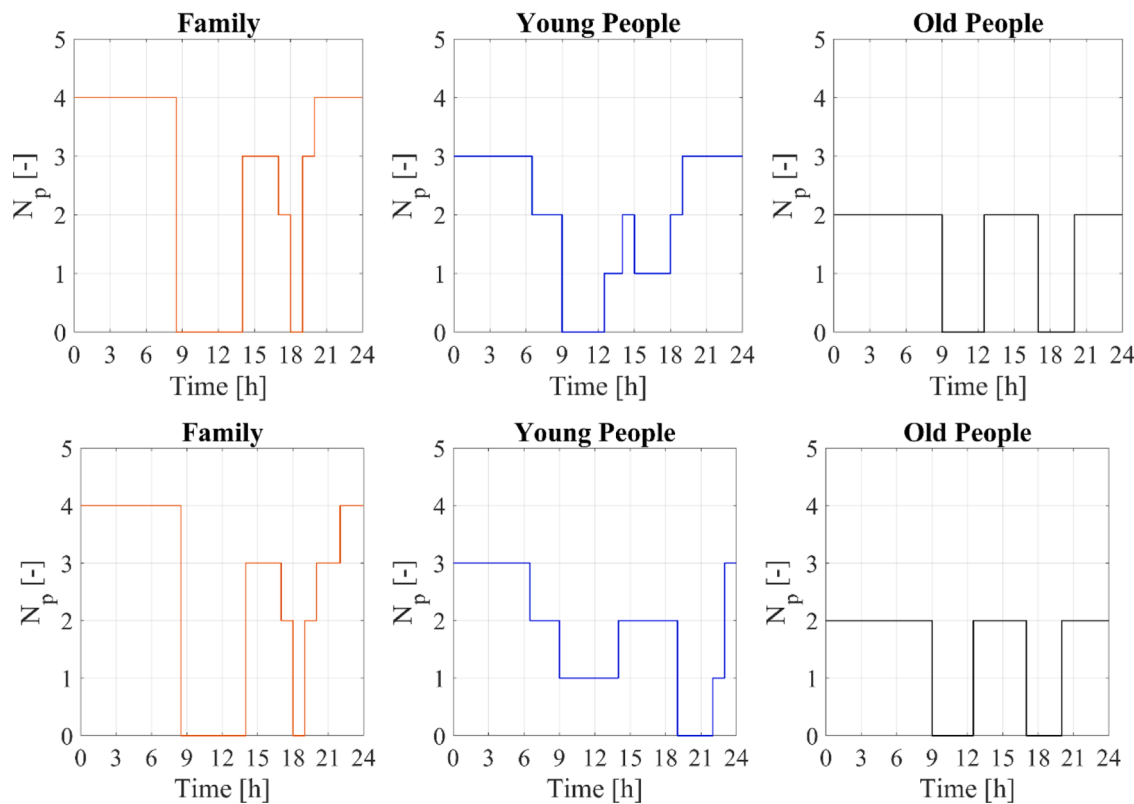


**Fig. 6.** Winter (above) and summer (below) scheduling of each kind of user for a single apartment: family (FAM), old people (OP) and young people (YP).

**Table 7**

Assumptions on the consumption and heat gain of electrical devices in the district (E. Air-Conditioning 1993).

Devices	Average power [kW]	Heat Gain [kW]	Radiative part [%]	Convective part [%]
Fridge	0.040	0.040	0	100
Dishwasher	1.820	0.364	51	34
Bakery	0.870	0.522	14	49
Cooking plane	1.500	0.900	24	16
TV	0.240	0.240	40	60
PC 3.5 GHz processor	0.090	0.090	10	90
16 GB ram				
Laptop	0.059	0.059	25	75
Washing machine	1270	0.254	40	60

decrease due to the increase of the temperature of the user H&C water loop and although  $T_{feed,NR1}$  begins to increase. This trend is also observed the rest of the day for the same reasons.

Finally, the maximum thermal energy provided by HPs-H&C ( $P_{th,HPs-H\&C}$ ) is found at 07:50 am, when all of the HPs are simultaneously activated and  $P_{th,HPs-H\&C}$  is equal to 6310 kW.

A similar trend is also detected for the HPs-H&C summer operation (Fig. 9). The 5<sup>th</sup> generation DHC network here allows the HPs-H&C to operate with COP between 5.85 and 6.65, values significantly higher than those of a conventional air-to-water HP operating in cooling mode. Similar to the winter case, this result is achieved with the lower condensation temperature with NR2 operating from 19°C to 23°C. It is

**Table 8**

Envelope features of each type of building.

Building element	Building A & B & C & D			
	U-value [W/m <sup>2</sup> K]	Thickness [m]	$\rho_s$ [-]	$\epsilon$ [-]
Roof	0.949	0.270	0.4	0.9
Facades	1.202-1.258	0.330-0.350		
Ground floor	1.115	0.400		
Adjacent ceiling	1.753	0.290		
Windows glass	2.89	0.004/0.016/0.004	0.13	0.18

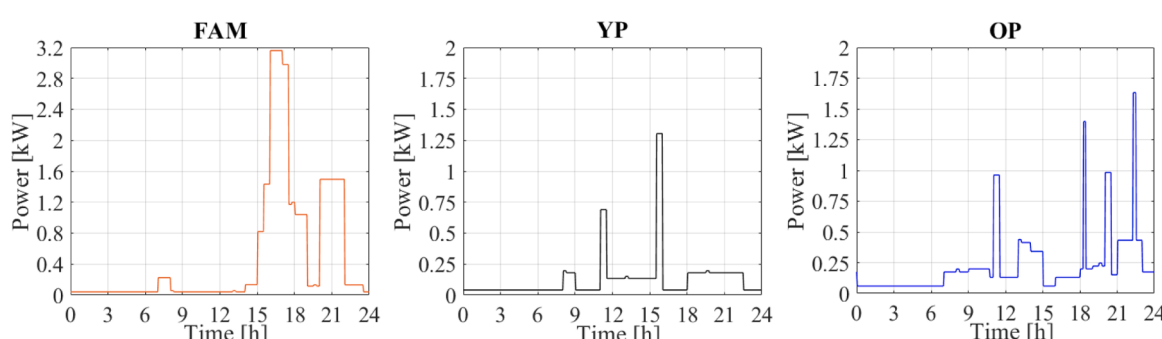


**Fig. 7.** Electricity load for each type of user: family (FAM), young people (YP) and old people (OP).

**Table 9**  
Design and operating parameters.

Component	Parameter	Description	Value	Unit
<b>PV</b>	$P_{max}$	Maximum power	290	W <sub>p</sub>
	$V_{oc}$	Open-circuit voltage	37.7	V
	$I_{sc}$	Short-circuit current	9.01	A
	$V_{mpp}$	Voltage at point of MPP	30.5	V
	$I_{mpp}$	Current at point of MPP	8.51	A
	$N_s$	Number modules in series	2	-
	$N_p$	Number modules in parallel	1096	-
	$A$	PV module area	1.6	m <sup>2</sup>
	$N_{cell}$	Number cells in series	15	-
	$\eta_{PV}$	Module efficiency	18	-
	$P_{rated,PV}$	PV panel rated power	2.51	MW
	$A_{PV}$	PV field area	160090	m <sup>2</sup>
	$P_{th,HP,heat}$	Rated heating capacity	1.25	MW <sub>th</sub>
	$P_{th,HP,cool}$	Rated cooling capacity	1.14	MW <sub>th</sub>
<b>HP</b>	$P_{th,GHP1s}$	Rated heating capacity	1.25	MW <sub>th</sub>
	$P_{th,GHP2s}$	Rated cooling capacity	1.14	MW <sub>th</sub>
	$COP$	Rated Coefficient of performance	4.67	-
	$EER$	Rated Energy efficiency ratio	5.10	-
	$m_{source}$	Rated water flow rate on source side	288.37	m <sup>3</sup> /h
	$m_{user}$	Rated water flow rate on user side	217.84	m <sup>3</sup> /h
	$T_{cond,C}$	Condenser design temperature during cooling operation	20-24	°C
	$T_{evap,H}$	Evaporator design temperature during heating operation	15-19	°C

well known that in cooling mode the COP increases for higher evaporation and lower condensation temperatures. From 06:00 to 07:06 am, the COP decreases from 6.61 to 5.85 because the  $T_{feed,NR2}$  increases from 20°C to 24°C. When  $T_{NR2}$  reaches the threshold value of 24°C, according to the control strategy of NR2, GHP2s are activated. When  $T_{feed,NR2}$  decreases to 20.5°C, from 07:06 to 08:15, the COP increases from 5.85 to 6.33. Despite the fact that  $T_{feed,NR2}$  decreases further, when it reaches 20°C the COP of the HPs-H&C begins to decrease, due to the decrease of users' H&C water loop temperature.

An increase of heating and cooling COPs reduces the electricity demand of the HPs. However, the overall balance must also consider the energy demanded by the GHPs. Fig. 10 shows that the heat exchange with the ground in GHP1s and GHP2s significantly enhances the performance of the HPs both during summer and winter operation. Specifically, the COP of GHP1s ranges between 4.81 and 5.02, values higher than those achieved with a conventional air-to-water HP. This can be attributed to the higher and more stable source temperature of the ground, compared to the air temperature. GHP2s results in a similar performance with its COP ranging between 7.20 and 7.50.

Fig. 11 shows the power on two representative winter and summer days. The photovoltaic power production ( $P_{el,PV}$ ) is related to the solar availability and becomes maximum at midday, with a peak of 2051 kW in winter and 2271 in summer. The power demand ( $P_{el,LOAD}$ ), on the other hand, is strongly affected by the occupancy scheduling of the buildings. The electricity demand increases in the afternoon and evening when most inhabitants of the district are home and use their electrical appliances. At that time HPs-H&C/HPs-DHW are in operation for meeting the required space H&C demand.  $P_{el,LOAD}$  includes the power delivered to the GHPs, the HPs-H&C and HPs-DHW, the auxiliary hydronic systems (i.e. pumps), lights, and the electrical appliances of the apartments. During a typical winter day, most of the electricity required by the district is taken from the grid. At the same time,  $P_{el,PV}$  exceeds  $P_{el,LOAD}$  at midday, leading to a peak of surplus power delivered to the grid equal to 1833 kW. A remarkable time shift between power production and demand is thus observed. This leads to large amounts of electricity imported and exported from/to the grid.

The misalignment between power production and power demand may constitute a significant challenge from the grid balancing point of view. Therefore, the installation of an electric energy storage system should be considered for improving the energy self-sufficiency of the

proposed plant and for improving the balance of the grid. Such a system would be able to store the surplus of renewable power (see Fig. 11) and reduce the amount of electricity imported/exported from/to the grid.

## 5.2. Monthly Results

Fig. 12 shows the thermal energy demand for building space heating ( $E_{th,heat}$ ) and building space cooling ( $E_{th,cool}$ ) of the selected residential district. In fact, the thermal energy demand for heating is significantly greater than that for cooling. This result is mainly related with the fact that the model of the residential district considers the self-shading of the buildings, which reduces the solar gain effecting the buildings.  $E_{th,cool}$  receives its maximum value of 369 MWh<sub>th</sub> in July, when the highest value of solar irradiance is seen.

Fig. 13 and Fig. 14 present the electric energy performance of the proposed DHC network. The electric energy demand of the plant ( $E_{el,LOAD}$ ) is maximum when the thermal energy demand of the district is maximum. This is due to the use of HPs that switch the thermal load of the district to an electric load. Therefore,  $E_{el,LOAD}$  is maximum from January to March, July to August and November to December, with values in the range of 599-770 MWh (Fig. 13). In winter, when  $E_{el,LOAD}$  is high and  $E_{el,PV}$  is low, the electric energy from the grid receives its maximum values (492-630 MWh).

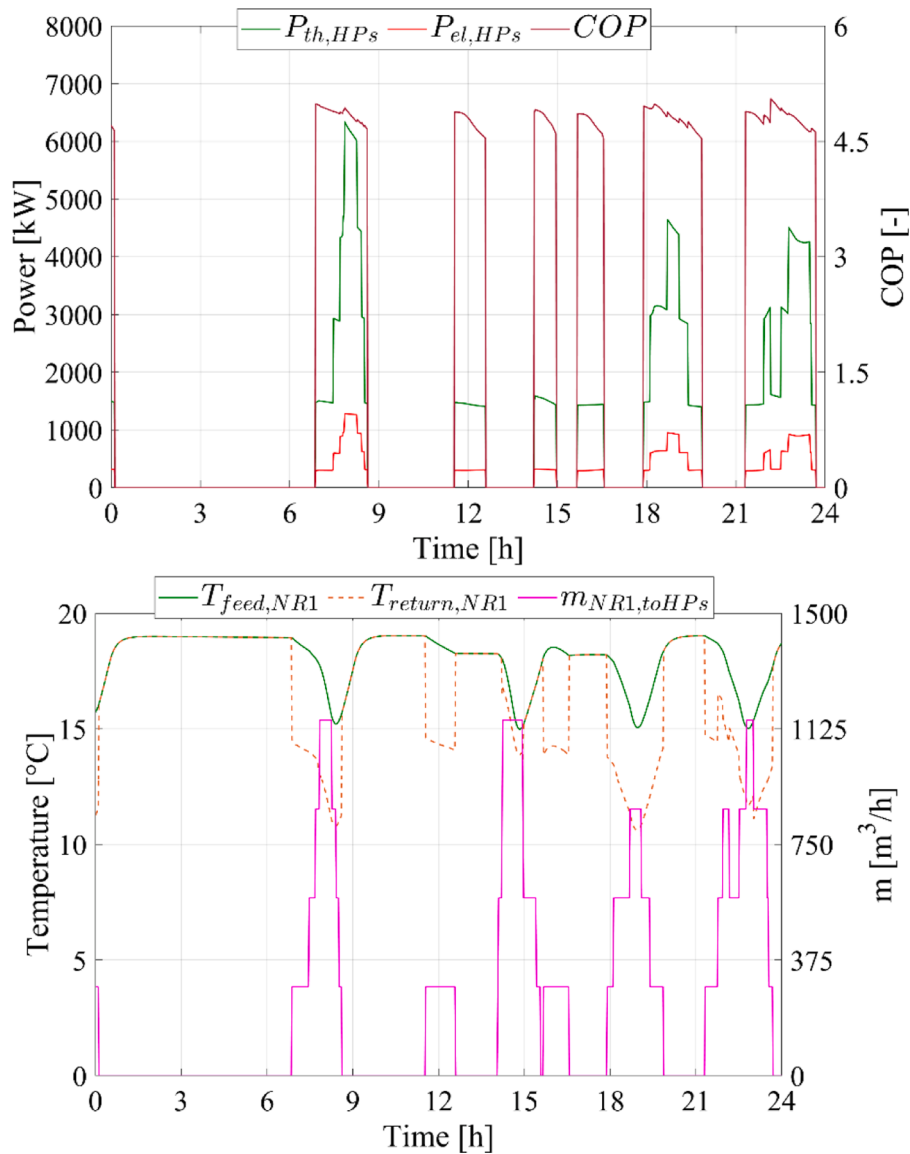
During the summer the self-consumed energy ( $E_{el,self}$ ) meets 37-43% of the electric energy demand of the proposed plant on average. During the remaining months the amount of electric energy demand of the district met by the photovoltaic energy reaches the minimum value of 14-20% in January and December (Fig. 14). Fig. 8 and Fig. 9 justify these results. During the winter solar irradiation is limited and the peak of power demand ( $P_{el,LOAD}$ ) occurs mainly in the late afternoon and in the evening. The system is thus not able to completely exploit the renewable power production ( $P_{el,PV}$ ) and most power demand is met by the grid ( $P_{el,fromGRID}$ ). On the other hand, the increased solar irradiation and power production in the afternoon during the summer allows for a better exploitation of the photovoltaic power production. Despite that, the peak of PV power production in the summer significantly exceeds the peak of power demand and the district is able to exploit only less than 46%  $E_{el,PV}$  (Fig. 14).

Fig. 15 displays the thermal energy performance of the ground heat exchangers GHE1 and GHE2. The thermal energy withdrawn by GHE1 ( $E_{th,GHE1}$ ) follows the same trend of  $E_{th,heat}$ . However,  $E_{th,GHE1}$  is never equal to zero, since NR1 also provides thermal energy to HPs-DHW that operate throughout the year to match the demand for DHW. The thermal energy discharged to the ground by GHE2 reaches its maximum value in July, when  $E_{th,GHE2}$  reaches the value of 456 MWh<sub>th</sub>.

Fig. 16 shows the energy performance of the recuperative heat exchanger M-HE that allows heat transfer between NR1 and NR2. In particular, Fig. 16 reports the energy ratios estimated with Eq. (17). The heat exchange between NR1 and NR2 occurs when heating and cooling demand exist at the same time, a situation not common for residential applications. During summer operation, NR2 withdraws thermal energy from the condensers of HPs-H&C operating in cooling mode and NR1 supplies thermal energy to the evaporators of the HPs-DHW. This allows NR1 to withdraw thermal energy from NR2. Fig. 16 clearly shows that due to the lower energy demand for DHW with respect to the thermal energy demand for building space cooling, this heat exchange contributes little to NR1 and NR2. The heat exchange in the M-HE is lower than 5.10% of the  $E_{th,toHPDHW}$ . Therefore, for this kind of application, the use of the M-HE must be checked from an economic point of view.

## 5.3. Annual Results

Table 10 summarizes the annual energy, environmental and economic performance of the selected residential district. This district is featured by an annual primary energy ( $PE_{RS}$ ) demand of 14.34 GWh at an annual operational cost of 1.30 M€/year. Table 11 reports the main



**Fig. 8.** Dynamic performance of HPs during winter operation.

performance indicators of the proposed renewable-assisted 5<sup>th</sup> generation DHC network.

As expected, the electric energy demand of the proposed system is significantly greater than the electric energy demand of the reference system, i.e., 7.01 GWh/year (PS) vs. 3.48 GWh/year (RS). This is due to the fact that the space heating and DHW demand of the residential district is matched by the 5<sup>th</sup> generation DHC network fed by electrically driven water-to-water HPs. Therefore, the thermal energy demand is switched into an electric load. Conversely, in the RS the thermal energy demand is matched with natural gas fired boilers. The PS, on the other hand, increases the electric consumption and eliminates, at the same time, the natural gas demand. The overall result is a roughly 10% reduction in primary energy demand for building space heating/cooling and DHW. This is related to the higher efficiency of the HPs, compared to conventional technologies. The efficiency of the HPs is further enhanced by the use of GHE and the low feeding temperature of the 5<sup>th</sup> generation DHC (Table 12). Similar results are obtained in the work presented by Bilardo et al. (Bilardo et al., 2021), where the modelling of a bidirectional low-temperature 5<sup>th</sup> generation DHC network coupled with reversible HPs for a nearly Zero Energy District is presented. In this work, the calculated coefficients of performance range between 4.06

and 6.23. However, as shown in the monthly results, the considered case study has a very limited simultaneity between space heating and cooling, limiting the use of the recuperative heat exchanger M-HE. In fact, the demand overlap coefficient (DOC see Eq.(18) and (Wirtz et al., 2020)) was equal to 0.03.

The overall plant, including the photovoltaic field, reaches very promising energy and environmental results, achieving a PES close to 64% and an avoided equivalent CO<sub>2</sub> emission index of 76%. The avoided equivalent CO<sub>2</sub> emissions obtained in the work of Wirtz et al. (Wirtz et al., 2020), where the analysis of a bidirectional 5<sup>th</sup> generation DH network is presented, are equal to 56%, when the designed system is compared to individual HVAC systems. The same value of the avoided equivalent CO<sub>2</sub> emission index, equal to 80%, is obtained in Ref. (Revesz et al., 2020), where a 5<sup>th</sup> generation DH ambient-temperature loop, integrating thermal, power and mobility energy vectors are presented.

From an economic point of view the proposed plant achieves a long SPB of 33 years, due to its high capital cost ( $C_{inv}$ ) equal to 11.27 M€. This value is common for this type of systems, because of the high capital costs for the associated network infrastructure, trenching of the pipe-work, drilling of boreholes and connection costs (Revesz et al., 2020).

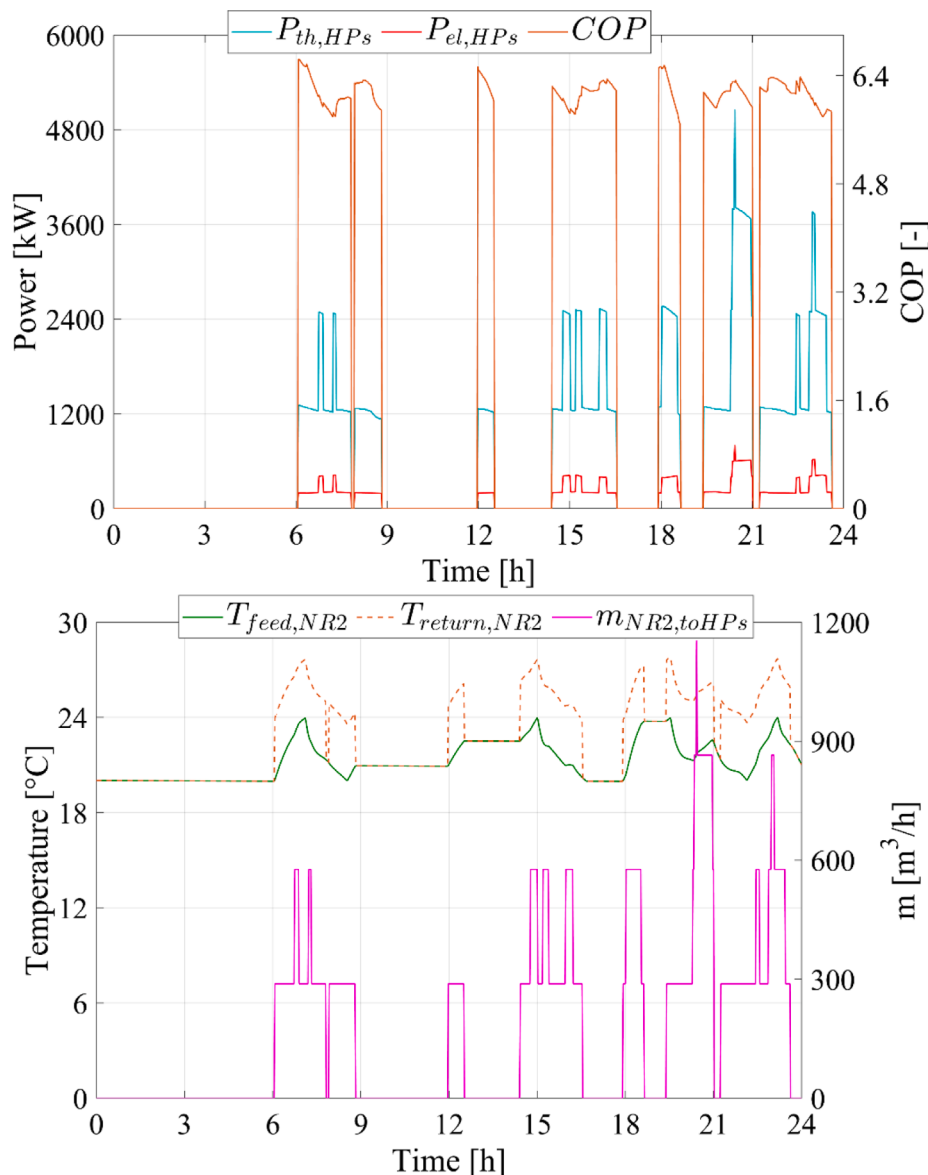


**Fig. 9.** Dynamic performance of the HPs during summer operation.

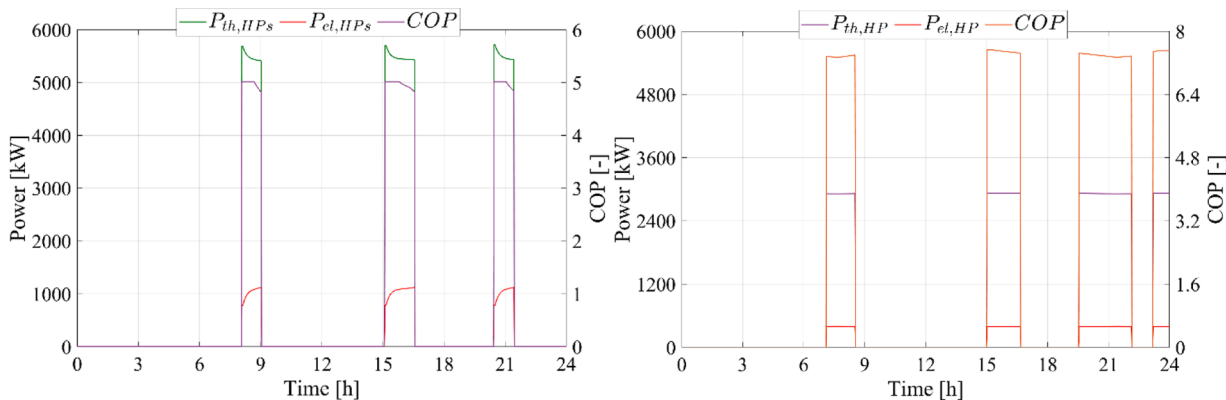


**Fig. 10.** Dynamic performance of i) GHP1s on a typical winter day (left); ii) GHP2s on a typical summer day (right).

**Table 13** summarizes the economic performance of the proposed plant. The simulated system achieves cost savings roughly equal to 34.7%. This agrees with reference (Wirtz et al., 2021), where cost savings between

10 % and 60 % were obtained for an optimized 5<sup>th</sup> generation DHC network including an air-source HP, compression chiller and thermal storage.

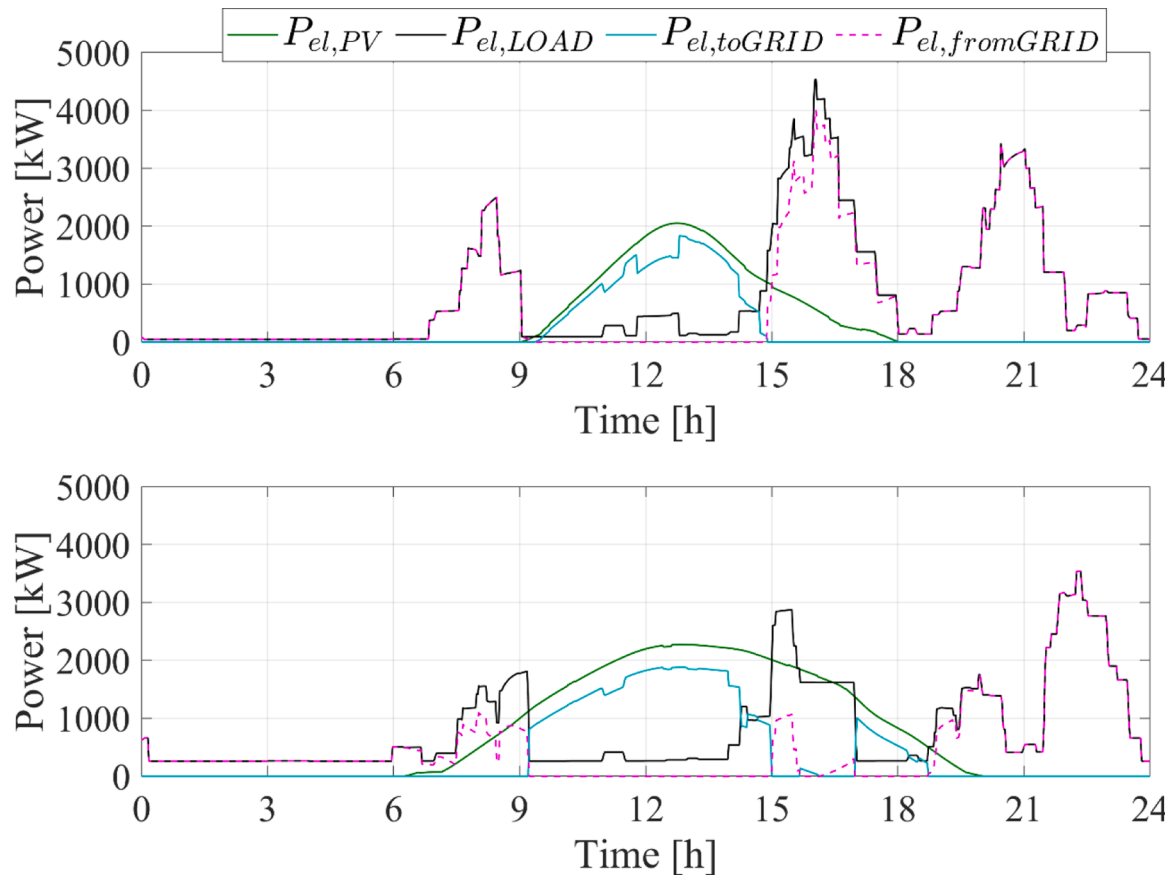


**Fig. 11.** Dynamic performance of the overall plant on a typical winter day (top) and on a typical summer day (bottom).

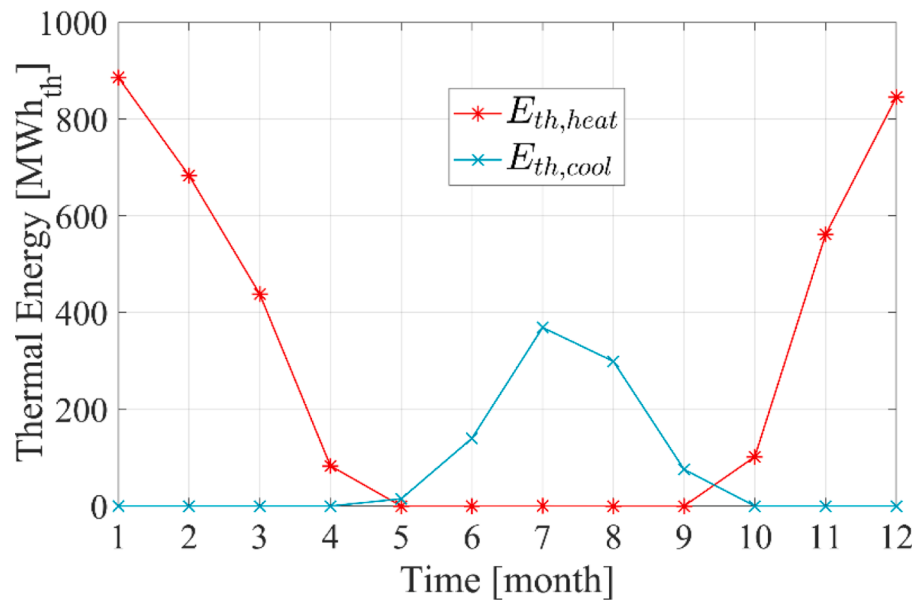


**Fig. 12.** Thermal Energy demand of the selected residential district in Leganes (Madrid).

**Fig. 15** shows the energy ratios of the photovoltaic performance. The system is seen to exploit only 47% of the electricity provided by the PV field. As explained previously, this is because the PV power production occurs mainly around midday, while the peak of power demand occurs mainly in the afternoon and the evening. For the same reasons the self-consumed energy meets only 30% of the electricity demand of the proposed 5<sup>th</sup> generation DHC network, **Fig. 17**.

#### 5.4. Parametric and Sensitivity analyses

A parametric analysis is carried out to detect which PV field capacity optimizes the environmental, economic and energy performance of the proposed 5<sup>th</sup> generation DHC network. The PV field area is varied from 9620 m<sup>2</sup> to 64102 m<sup>2</sup>, i.e.,  $P_{el,PV,rated}$  from 1.5 MW to 10 MW. To analyze how the purchasing price of energy effects the economic performance of

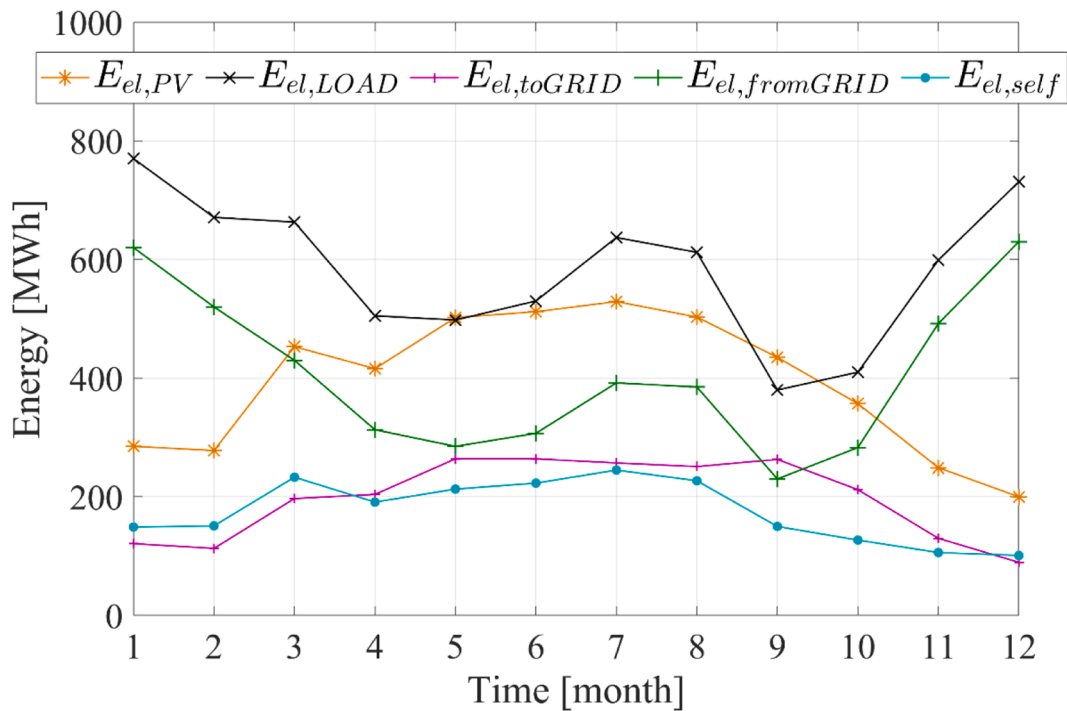


Fig. 13. Electric energy performance of the proposed solar-assisted 5<sup>th</sup> generation DHC.

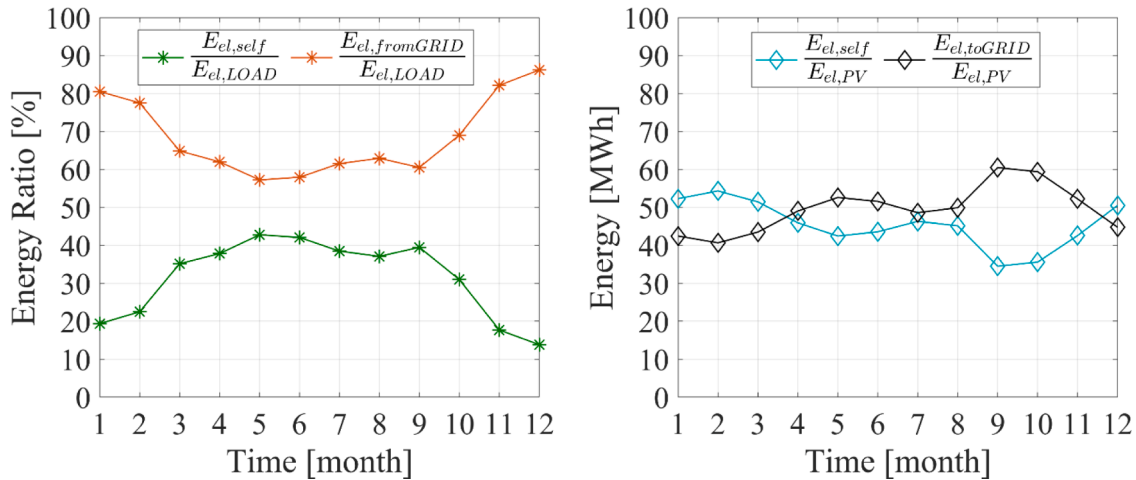


Fig. 14. Electric energy ratios of the proposed renewable-assisted 5<sup>th</sup> generation DHC.

the proposed system two sensitivity analyses are carried out: i) variation of the purchasing cost of electricity ( $J_{el,fromGRID}$ ) from 0.05 €/kWh to 0.35 €/kWh, and ii) variation of the purchasing cost of natural gas from 0.20 €/Sm<sup>3</sup> to 1.50 €/Sm<sup>3</sup>.

#### 5.4.1. Parametric analysis: PV area

As expected, the increase of the PV field area ( $A_{PV}$ ) leads to an increase of the PES and  $\Delta CO_2$ . Increasing the PV area from 9620 m<sup>2</sup> to 64100 m<sup>2</sup> leads to an increase of the PES from 38% to 256%, Fig. 18. An increase of the PV area causes an increase of the renewable electricity production of the plant. However, despite the dramatic increase of the electric energy production, the renewable electric energy can meet only a limited share of the electricity demand of the plant. In particular, increasing  $A_{PV}$  from 9620 m<sup>2</sup> to 64100 m<sup>2</sup> the ratio  $E_{el,self}/E_{el,LOAD}$  rises from 22% to 47%, Fig. 19. The PV power production takes place around midday, whereas the power demand mainly occurs in the late afternoon and evening. Therefore, the increase of the PV area, i.e., of the rated PV

field capacity, leads only to an increase of the power production mainly in the hours when the power demand is limited. Thus, the increase of the  $A_{PV}$  size leads only to a limited increase of the self-consumed energy, and it does not enable the plant to completely exploit the produced renewable power. As consequence, increasing  $A_{PV}$  from 9620 m<sup>2</sup> to 64100 m<sup>2</sup> increases the surplus electricity delivered to the grid and ranges between 44% and 83% of the energy produced in the PV field, Fig. 19. However, this aspect improves the economic annual economic savings ( $\Delta C$ ) of the plant, because of the electricity exported to the grid. The SPB also decreases to 15.38 years when  $A_{PV}$  is equal to 64100 m<sup>2</sup>, Fig. 20. From an economic point of view thus the economic performance of the proposed plant is enhanced overall, with the capital cost ( $C_{inv}$ ) growth due to  $A_{PV}$  increase balanced by the increase of the  $\Delta C$ .

#### 5.4.2. Sensitivity analysis: purchasing cost of electricity and natural gas

Fig. 21 displays the sensitivity analysis of the purchasing cost of electricity and natural gas. Since the 5<sup>th</sup> generation DHC network is

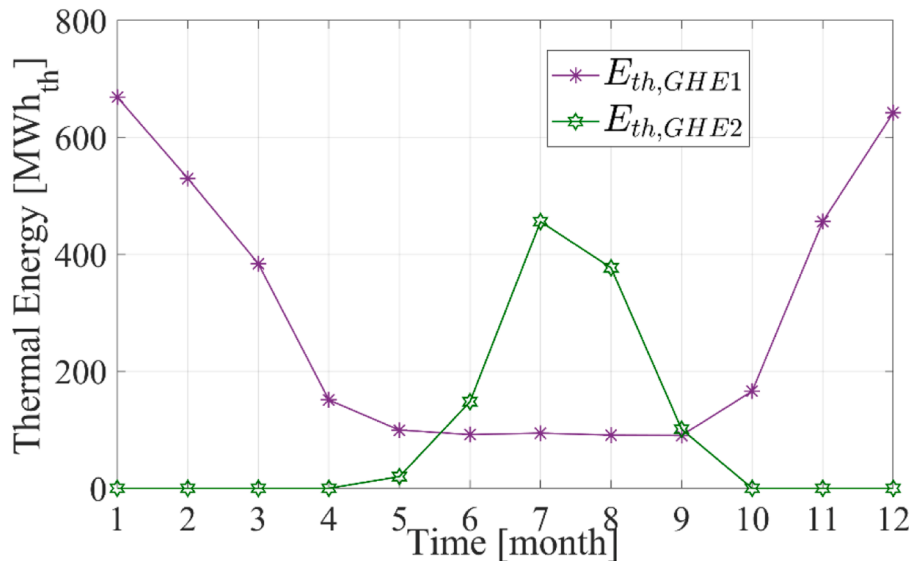


Fig. 15. Thermal energy performance of GHE.

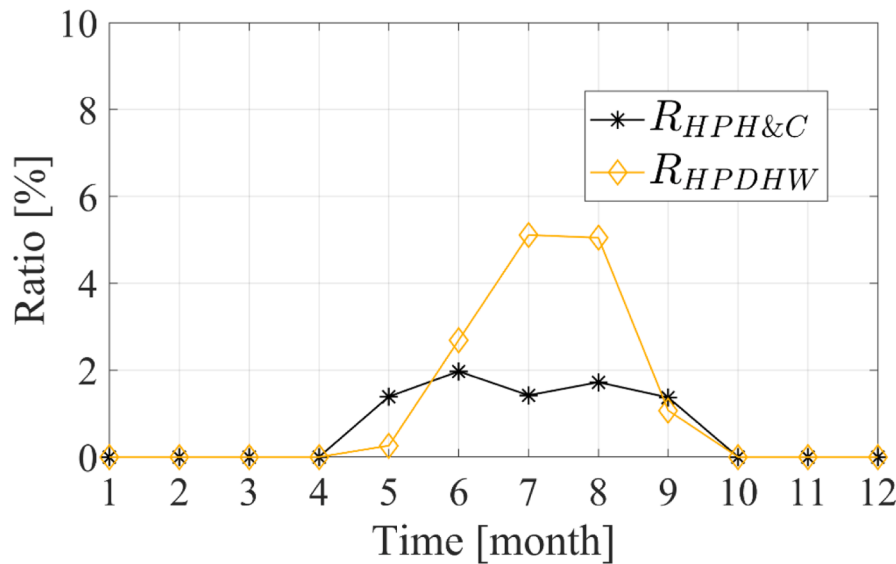


Fig. 16. M-HE energy performance.

Table 10

Residential district energy, economic and environmental performance.

$E_{th,heat}$	$E_{th,cool}$	$E_{el,LOAD}$	$PE_{RS}$	$V_{NG}$	$C_{RS}$	$CO_2$
3.60	0.90	3.48	14.34	694741.90	1.32	1988

based on electrically driven water-to-water HPs, converting the thermal energy demand of the district into electricity demand, the increase of the purchasing cost of electricity ( $J_{el,fromGRID}$ ) dramatically worsens the economic performance of the proposed system. However, the SPB decreases to 24 year when  $J_{el,fromGRID}$  decreases to 0.10 €/kWh.

The increase of the purchasing cost of natural gas ( $J_{NG}$ ), on the other hand, enhances the economic performance of the proposed system remarkably, for the same reason previously explained. In fact, the increase of  $J_{NG}$  leads to an increase of the operational cost of the RS and improves the economic savings of the PS. The SPB decreases to 16 years when  $J_{NG}$  is equal to 1.20 €/Sm<sup>3</sup>. As expected, the reduction of the cost of natural gas makes the proposed 5<sup>th</sup> generation DHC network not

Table 11

Energy and environmental performance of the proposed 5<sup>th</sup> generation DHC network.

Parameter	Value	Unit
$E_{el,LOAD}$	7.01	GWh/year
$E_{el,district}$	3.48	
$E_{el,pump}$	1.29	
$E_{el,HPs}$	2.24	
$PE_{5thgen}$	7.08	
$E_{el,PV}$	4.72	
$E_{el,toGRID}$	2.37	
$E_{el,fromGRID}$	4.89	
$E_{el,self}$	2.12	
$PE_{PS}$	5.06	
$\Delta PE$	8.95	%
$PES$	63.87	
$PES_{5thDHC}$	9.99	
$\Delta CO_2$	1472.81	t/year
$\Delta CO_2$	76.25	%
$\Phi$	0.03	

**Table 12**

Performance indices of the HPs of the 5<sup>th</sup> generation DHC network.

COP <sub>HPDHW</sub>	COP <sub>HPs-H&amp;C</sub>	EER <sub>HPs-H&amp;C</sub>	COP <sub>GHP1s</sub>	COP <sub>GHP2s</sub>
4.58	4.92	6.10	5.31	7.45

**Table 13**

Economic performance of the proposed network.

<i>C<sub>inv</sub></i>	<i>C<sub>PS</sub></i>	$\Delta C$	<i>SPB</i>	<i>NPV</i>	<i>PI</i>
M€ 11.27	M€/year 0.98	M€/year 0.34	years 33.18	M€ -6.56	-0.58

profitable.

## 6. Conclusions

This work presents the simulation and evaluation of a solar-assisted 5<sup>th</sup> generation district heating and cooling network based on water-to-water heat pumps, ground heat pumps and a photovoltaic field. The network is a bidirectional low-temperature network based on a cold and warm ring. The main findings of this work are the following:

- The network improves the performance significantly, with the water-to-water heat pumps meeting the thermal demand of the residential district with coefficients of performance greater than the rated ones.
- The adoption of the ground as thermal energy source is a promising solution, able to significantly enhance the energy performance of heat pumps.

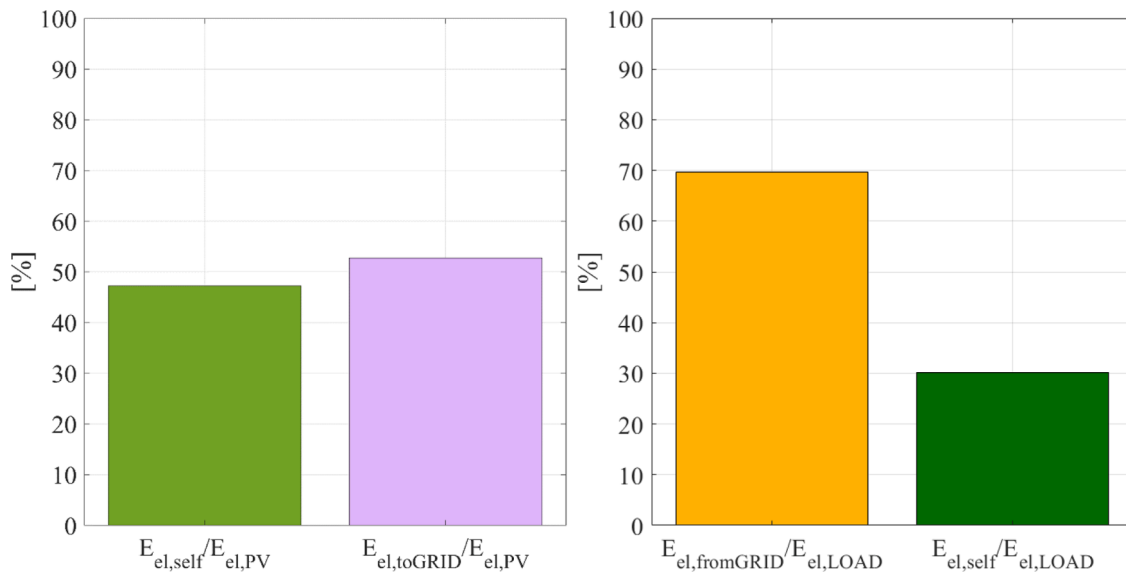


Fig. 17. Annual energy ratio.

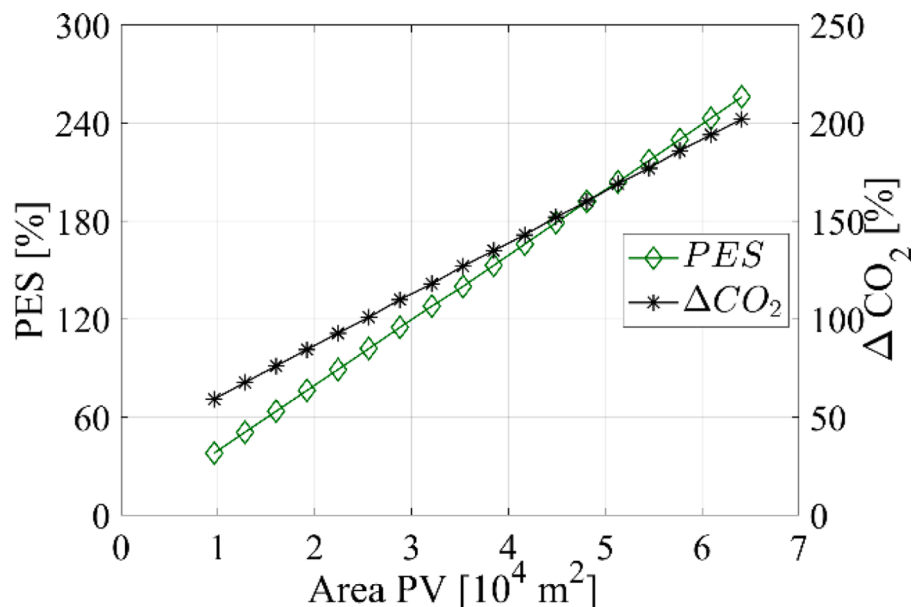


Fig. 18. Parametric analysis of the PES and  $\Delta CO_2$ .

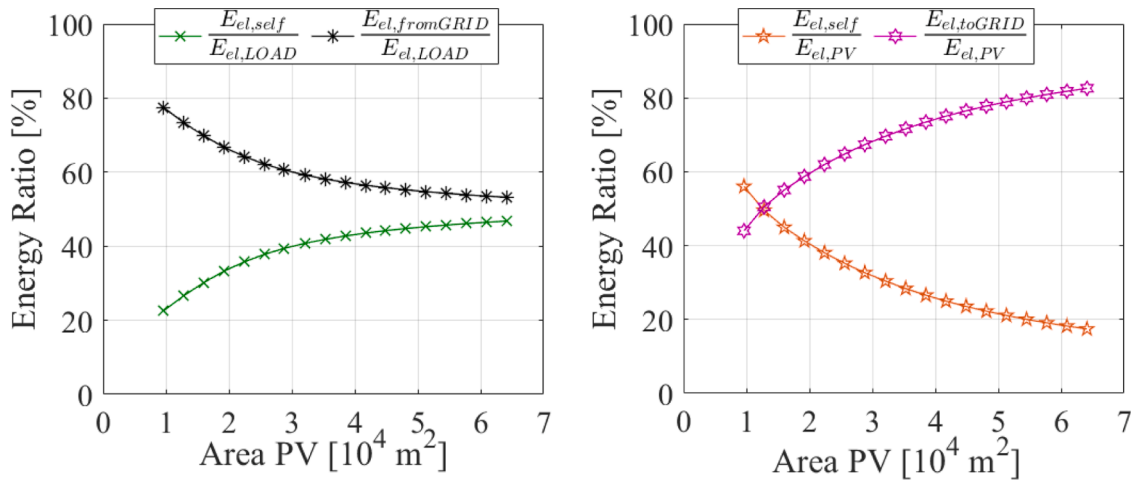


Fig. 19. Parametric analysis of the energy ratio.

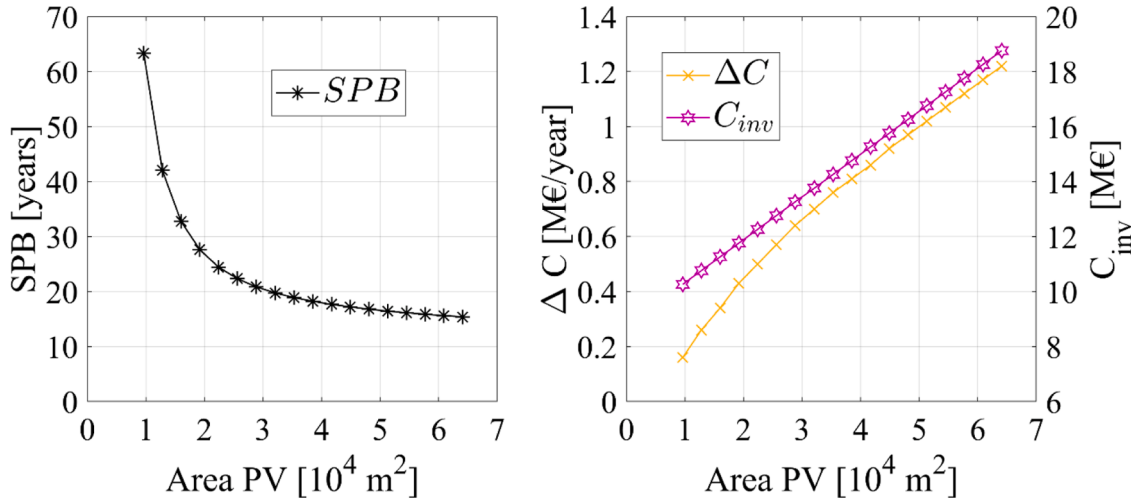


Fig. 20. Parametric analysis of the economic results.

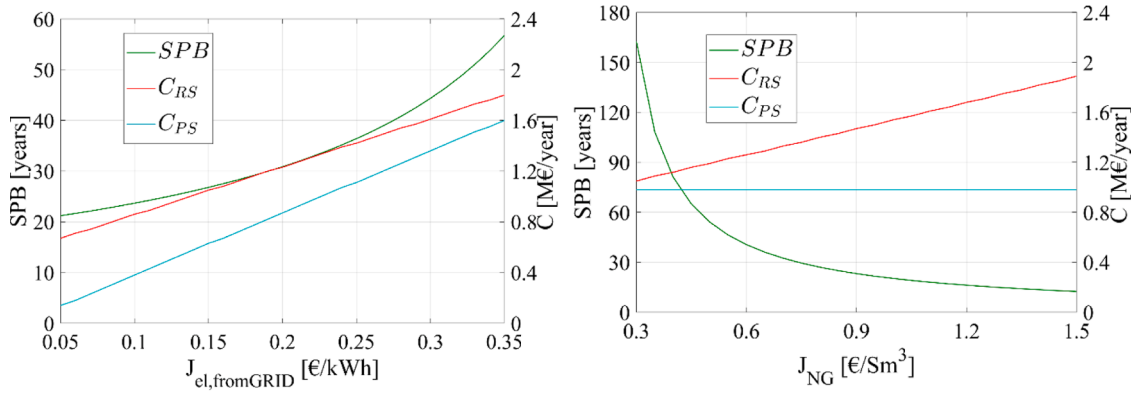


Fig. 21. Sensitivity analysis: purchasing cost of electricity (left) and natural gas (right).

- The adoption of a 5<sup>th</sup> generation network based on heat pumps switches the thermal load into an electric load. For the analyzed case study, the load is mainly located in the late afternoon and evening limiting the advantage of coupling the network with a photovoltaic field. The detected misalignment between power production and power demand may lead to a critical management issue of the local grid. The installation of an energy storage system, not considered

here, could avert grid balancing issues and improve the energy performance of the renewable-based system proposed. In addition, a thermal energy storage, centralized or decentralized, could shift the peak of power demand for HP activation to hours of higher solar availability.

- The adoption of the proposed 5<sup>th</sup> generation district heating and cooling network leads to a 10% reduction of the primary energy

employed for building space heating and cooling and domestic hot water in the studied district. This relatively conservative result is due to the limited simultaneity between heating and cooling demand. The inclusion of other kinds of users (e.g., commercial users, hospitals, server farm/data centres) could increase the simultaneity between heating and cooling demand that would, in turn, significantly improve the energy performance of the network.

- The installation of a photovoltaic field of 2.51 MW is considered to meet the power demand of the system. The renewable system has promising energy and environmental results, achieving a primary energy saving index of 64 % and reducing the CO<sub>2</sub> emissions by 76%. Despite these promising results, the network cannot fully exploit the renewable electricity produced and only 30% of its direct electricity demand is met by the photovoltaic field.
- The economic results result in the very high payback period of 33 years. This is related to the high cost of the proposed system, which involves excavation costs, pipe laying, heat pumps installation etc.
- Since the adoption of the 5<sup>th</sup> generation district heating and cooling network converts the thermal load into an electric load, the increase of the purchasing cost of electricity worsens the economic performance of the system. For the same reason, an increase in the purchasing cost of natural gas would remarkably improve its economic performance.

Overall, the proposed 5th generation district heating and cooling network based on water-to-water heat pumps, ground heat pumps and a photovoltaic field is a promising solution for reducing the environmental impact of the chosen residential district. However, in order to increase the benefits of such a novel district heating and cooling network, other kinds of thermal energy consumers should be included and linked to the network to increase the contemporaneity between cooling and heating demand. Lastly, in order to remarkably enhance the ability of the proposed system to exploit the renewable power produced by the photovoltaic field an energy storage system should be installed. This would also reduce the peak of surplus power delivered to the local grid, which may damage the local grid.

## Declaration of Competing Interest

None.

## Acknowledgment

Fontina Petrakopoulou would like to thank the Spanish Ministry of Science, Innovation and Universities and the Universidad Carlos III de Madrid (Ramón y Cajal Programme, RYC-2016-20971).

## References

- Abokersh, M. H., et al. (2020). Flexible heat pump integration to improve sustainable transition toward 4th generation district heating. *Energy Conversion and Management*, 225, Article 113379.
- Abugabbara, M., et al. (2020). Bibliographic analysis of the recent advancements in modeling and co-simulating the fifth-generation district heating and cooling systems. *Energy and Buildings*, 224, Article 110260.
- Aditya, G. R., et al. (2020). Comparative costs of ground source heat pump systems against other forms of heating and cooling for different climatic conditions. *Sustainable Energy Technologies and Assessments*, 42, Article 100824.
- Aermec. 2020; Available from: <https://global.aermec.com/it/>.
- Allen, A., et al. (2020). Evaluation of low-energy heating and cooling systems and topology optimization for deep energy savings at the urban district level. *Energy Conversion and Management*, 222, Article 113106.
- Arriazu-Ramos, A., et al. (2021). Difficulties in the energy renovation processes of district heating buildings. Two case studies in a temperate climate. *Sustainable Cities and Society*, 75, Article 103246.
- ASHRAE. A. (2005). *Handbook of fundamentals*. Atlanta, GA: American Society of Heating Refrigerating and Air Conditioning Engineers.
- Büning, F., et al. (2018). Bidirectional low temperature district energy systems with agent-based control: Performance comparison and operation optimization. *Applied Energy*, 209, 502–515.
- Buffalo, M., et al., Modelling a fifth-generation bidirectional low temperature district heating and cooling (5GDHC) network for nearly Zero Energy District (nZED). *Energy Reports*, 2021.
- Buffa, S., et al. (2019). 5th generation district heating and cooling systems: A review of existing cases in Europe. *Renewable and Sustainable Energy Reviews*, 104, 504–522.
- Buonomano, A., Calise, F., & Ferruzzi, G. (2013). THERMOECONOMIC ANALYSIS OF STORAGE SYSTEMS FOR SOLAR HEATING AND COOLING SYSTEMS: A COMPARISON BETWEEN VARIABLE-VOLUME AND FIXED-VOLUME TANKS. *Energy*, 59, 600–616.
- Buonomano, A., et al. (2016). BIPVT systems for residential applications: An energy and economic analysis for European climates. *Applied Energy*, 184, 1411–1431.
- Buonomano, A., et al. (2018). A hybrid renewable system based on wind and solar energy coupled with an electrical storage: Dynamic simulation and economic assessment. *Energy*, 155, 174–189.
- Calise, F., et al. (2019). A novel paradigm for a sustainable mobility based on electric vehicles, photovoltaic panels and electric energy storage systems: Case studies for Naples and Salerno (Italy). *Renewable and Sustainable Energy Reviews*, 111, 97–114.
- Calise, F., et al. (2020). Dynamic simulation, energy and economic comparison between BIPV and BIPVT collectors coupled with micro-wind turbines. *Energy*, 191, Article 116439.
- Calise, F., et al. (2020). Water-energy nexus: A thermoeconomic analysis of polygeneration systems for small Mediterranean islands. *Energy Conversion and Management*, 220, Article 113043.
- Calise, F., et al. (2020). Energy and economic analysis of a small hybrid solar-geothermal trigeneration system: A dynamic approach. *Energy*, 208, Article 118295.
- Calise, F., et al. (2020). Energy efficiency in small districts: Dynamic simulation and technoeconomic analysis. *Energy Conversion and Management*, 220, Article 113022.
- Calise, F. (2010). Thermoeconomic analysis and optimization of high efficiency solar heating and cooling systems for different Italian school buildings and climates. *Energy and Buildings*, 42(7), 992–1003.
- Calixto, S., Cozzini, M., & Manzolini, G. (2021). Modelling of an Existing Neutral Temperature District Heating Network: Detailed and Approximate Approaches. *Energy*, 14(2).
- Carotenuto, A., Figaj, R. D., & Vanoli, L. (2017). A novel solar-geothermal district heating, cooling and domestic hot water system: Dynamic simulation and energy-economic analysis. *Energy*, 141, 2652–2669.
- Casquero-Modrego, N., & Goñi-Modrego, M. (2019). Energy retrofit of an existing affordable building envelope in Spain, case study. *Sustainable Cities and Society*, 44, 395–405.
- Chen, Y., et al. (2021). Integrated performance analysis of a space heating system assisted by photovoltaic/thermal collectors and ground source heat pump for hotel and office building types. *Renewable Energy*, 169, 925–934.
- Commission, E. 2020; Available from: [https://ec.europa.eu/info/strategy/priorities-2019-2024/european-green-deal\\_en](https://ec.europa.eu/info/strategy/priorities-2019-2024/european-green-deal_en).
- Dénarié, A., et al. (2019). Industrial excess heat recovery in district heating: Data assessment methodology and application to a real case study in Milano. *Italy. Energy*, 166, 170–182.
- American Society of Heating, R., E. Air-Conditioning. (1993). *1993 ASHRAE handbook: fundamentals*. Atlanta, GA: ASHRAE.
- Eicker, U. (2018). *URBAN ENERGY SYSTEMS FOR LOW-CARBON CITIES*. Academic Press.
- Fabre, A., et al. (2018). Dynamic modeling for evaluation of triple-pipe configuration potential in geothermal district heating networks. *Energy Conversion and Management*, 173, 461–469.
- GIORDANO, I. 2020; Available from: <http://www.idraulicagiordano.it/>.
- Gu, J., et al. (2019). Analysis of a hybrid control scheme in the district heating system with distributed variable speed pumps. *Sustainable Cities and Society*, 48, Article 101591.
- Hammar, T., & Levihn, F. (2020). Time-dependent climate impact of biomass use in a fourth generation district heating system, including BECCS. *Biomass and Bioenergy*, 138, Article 105606.
- Han, J., et al. (2021). Analysis of thermal performance and economy of ground source heat pump system: a case study of the large building. *Geothermics*, 89, Article 101929.
- Handbook, A. (1996). *HVAC systems and equipment*, 39. : Chapter.
- Harney, P., Gartland, D., & Murphy, F. (2020). Determining the optimum low-temperature district heating network design for a secondary network supplying a low-energy-use apartment block in Ireland. *Energy*, 192, Article 116595.
- Instituto Nacional de Estadística.
- International Energy Agency - IEA. 2015, Energy Climateand Change - World Energy Outlook Special Report. Special Report on Energy and Climate Change on [iea.org/](http://iea.org/) publications website visited on February 2016.
- Ivezic, D., et al. (2020). Assessments of effects of implementation of strategic plans for development of Belgrade District heating system. *Sustainable Cities and Society*, 61, Article 102304.
- Karamanos, P. (1997). COGENERATION AND DISTRICT HEATING: CONSTRAINTS AND OPPORTUNITIES. *The Journal of Energy and Development*, 22(2), 245–274.
- Khosravi, A., et al. (2021). Waste heat recovery from a data centre and 5G smart poles for low-temperature district heating network. *Energy*, 218, Article 119468.
- Klein S.A., B.W.A., Mitchell J.W., Duffie J.A., Duffie N.A., Freeman T.L., et al., Solar energy laboratory, TRNSYS. A transient system simulation program. 2006.
- Leganes ayuntamiento.
- Lu, M., et al. (2021). Operational optimization of district heating system based on an integrated model in TRNSYS. *Energy and Buildings*, 230, Article 110538.
- Lund, H., et al. (2021). Perspectives on fourth and fifth generation district heating. *Energy*, 227, Article 120520.
- Mahmoud, M., et al. (2020). Recent advances in district energy systems: A review. *Thermal Science and Engineering Progress*, 20, Article 100678.

- Maximov, S. A., Mehmood, S., & Friedrich, D. (2021). Multi-objective optimisation of a solar district heating network with seasonal storage for conditions in cities of southern Chile. *Sustainable Cities and Society*, 73, Article 103087.
- Mei, V. C. (1986). *HORIZONTAL GROUND-COIL HEAT EXCHANGER THEORETICAL AND EXPERIMENTAL ANALYSIS*. TN (USA): Oak Ridge National Lab.
- Millar, M.-A., et al. (2021). Identification of key performance indicators and complimentary load profiles for 5th generation district energy networks. *Applied Energy*, 291, Article 116672.
- Murray, M. C., et al. (2009). Live Energy Trnsys -Trnsys Simulation within Google Sketchup. In *Eleventh International IBPSA Conference*. Glasgow, Scotland July 27-30.
- Neymark, J. and R. Judkoff, International Energy Agency building energy simulation test and diagnostic method (IEA BESTEST) – in-depth diagnostic cases for ground coupled heat transfer related to slab-on-grade construction. Technical Report NREL/TP-550-43388. Available from: <http://www.nrel.gov/docs/fy08osti/43388.pdf>. 2008.
- Nielsen, S., et al. (2020). Unconventional excess heat sources for district heating in a national energy system context. *Energies*, 13(19).
- Nielsen, T. B., et al. (2021). Perspectives on energy efficiency and smart energy systems from the 5th SESAAU2019 conference. *Energy*, 216, Article 119260.
- Pérez-Lombard, L., Ortiz, J., & Pout, C. (2008). A review on buildings energy consumption information. *Energy and Buildings*, 40(3), 394–398.
- Pellegrini, M., & Bianchini, A. (2018). The Innovative Concept of Cold District Heating Networks: A Literature Review. *Energies*, 11(1).
- Piemonte, R., [http://www.regione.piemonte.it/oopp/prezzario/dwd/2018/Prezzario\\_Regione\\_Piemonte\\_2018.pdf](http://www.regione.piemonte.it/oopp/prezzario/dwd/2018/Prezzario_Regione_Piemonte_2018.pdf). 2018, [http://www.regione.piemonte.it/oopp/prezzario/dwd/2018/Prezzario\\_Regione\\_Piemonte\\_2018.pdf](http://www.regione.piemonte.it/oopp/prezzario/dwd/2018/Prezzario_Regione_Piemonte_2018.pdf).
- Revesz, A., et al. (2020). Developing novel 5th generation district energy networks. *Energy*, 201, Article 117389.
- Rezaie, B., & Rosen, M. A. (2012). District heating and cooling: Review of technology and potential enhancements. *Applied Energy*, 93, 2–10.
- Romanchenko, D., et al. (2021). Impacts of demand response from buildings and centralized thermal energy storage on district heating systems. *Sustainable Cities and Society*, 64, Article 102510.
- Ruesch, F., & Evins, R. (2014). District heating and cooling with low temperature networkssketch of an optimization problem. In *Proceedings of the COLEB 2014 workshop on computational optimisation of low-energy buildings*.
- SALMSON, <http://www.salmson.com/index.php?id=19&L=2>, Editor. 2019.
- Saloux, E., & Candaleno, J. A. (2020). Optimal rule-based control for the management of thermal energy storage in a Canadian solar district heating system. *Solar Energy*, 207, 1191–1201.
- Sameti, M., & Haghhighat, F. (2019). Optimization of 4th generation distributed district heating system: Design and planning of combined heat and power. *Renewable Energy*, 130, 371–387.
- Sandvall, A., Hagberg, M., & Lygnerud, K. (2021). Modelling of urban excess heat use in district heating systems. *Energy Strategy Reviews*, 33, Article 100594.
- Sinha, S., & Chandel, S. S. (2015). Prospects of solar photovoltaic-micro-wind based hybrid power systems in western Himalayan state of Himachal Pradesh in India. *Energy Conversion and Management*, 105, 1340–1351.
- Sommer, T., et al. (2020). The reservoir network: A new network topology for district heating and cooling. *Energy*, 199, Article 117418.
- Tapia, C., et al. (2017). Profiling urban vulnerabilities to climate change: An indicator-based vulnerability assessment for European cities. *Ecological Indicators*, 78, 142–155.
- Tian, Z., et al. (2019). Large-scale solar district heating plants in Danish smart thermal grid: Developments and recent trends. *Energy Conversion and Management*, 189, 67–80.
- Todorov, O., et al. (2020). A method and analysis of aquifer thermal energy storage (ATES) system for district heating and cooling: A case study in Finland. *Sustainable Cities and Society*, 53, Article 101977.
- TRNSYS, TRAnsnient System Simulation program. Vol. 4 - Mathematical Reference.
- von Rhein, J., et al. (2019). Development of a topology analysis tool for fifth-generation district heating and cooling networks. *Energy Conversion and Management*, 196, 705–716.
- Wahlroos, M., et al. (2017). Utilizing data center waste heat in district heating – Impacts on energy efficiency and prospects for low-temperature district heating networks. *Energy*, 140, 1228–1238.
- Wirtz, M., et al. (2020). 5th Generation District Heating: A novel design approach based on mathematical optimization. *Applied Energy*, 260, Article 114158.
- Wirtz, M., et al. (2020). Quantifying Demand Balancing in Bidirectional Low Temperature Networks. *Energy and Buildings*, 224, Article 110245.
- Wirtz, M., et al. (2021). Temperature control in 5th generation district heating and cooling networks: An MILP-based operation optimization. *Applied Energy*, 288, Article 116608.
- Xu, Q., et al. (2021). A new type of two-supply, one-return, triple pipe-structured heat loss model based on a low temperature district heating system. *Energy*, 218, Article 119569.
- Yang, S., & Lee, S. B. (2020). Dynamic thermal analysis of a residential ground-source heat pump. *Sustainable Energy Technologies and Assessments*, 37, Article 100608.
- Ye, B., et al. (2021). Research on quantitative assessment of climate change risk at an urban scale: Review of recent progress and outlook of future direction. *Renewable and Sustainable Energy Reviews*, 135, Article 110415.
- Zajacs, A., & Borodijecs, A. (2019). Assessment of development scenarios of district heating systems. *Sustainable Cities and Society*, 48, Article 101540.
- Zarin Pass, R., Wetter, M., & Piette, M. A. (2018). A thermodynamic analysis of a novel bidirectional district heating and cooling network. *Energy*, 144, 20–30.
- Zhou, K., et al. (2020). Performance assessment and techno-economic optimization of ground source heat pump for residential heating and cooling: A case study of Nanjing, China. *Sustainable Energy Technologies and Assessments*, 40, Article 100782.